DOT/FAA/AR-03/21

Office of Aviation Research
Washington, D.C. 20591

Characterization of In-Plane, Shear-Loaded Adhesive Lap Joints: Experiments and Analysis

May 2003

Final Report

This document is available to the U.S. public through the National Technical Information Service (NTIS), Springfield, Virginia 22161.

U.S. Department of Transportation
Federal Aviation Administration

NOTICE

Technical Report Documentation Page

1. Report No.	2. Government Accession No.	3. Recipient's Catalog No.
DOT/FAA/AR-03/21		

4. Title and Subtitle	5. Report Date
CHARACTERIZATION OF IN-PLANE, SHEAR-LOADED ADHESIVE LAP JOINTS: EXPERIMENTS AND ANALYSIS	May 2003
	6. Performing Organization Code

7. Author(s)	8. Performing Organization Report No.
John Tomblin,[†] Waruna Seneviratne,[†] Hyonny Kim,[*] and Jungmin Lee[*]	

9. Performing Organization Name and Address		10. Work Unit No. (TRAIS)
[†]Department of Aerospace Engineering Wichita State University Wichita, KS 67260-0093	[*]School of Aeronautics and Astronautics Purdue University West Lafayette, IN 47907-1282	11. Contract or Grant No. 00-C-WSU-00-007

12. Sponsoring Agency Name and Address	13. Type of Report and Period Covered
U.S. Department of Transportation Federal Aviation Administration Office of Aviation Research Washington, DC 20591	Final Report
	14. Sponsoring Agency Code ACE-120

15. Supplementary Notes

The FAA William J. Hughes Technical Center Technical Monitor was Peter Shyprykevich.

16. Abstract

The growing applications of adhesive bonding in aircraft structures requires more emphasis be placed on analytical models to predict failure and load carrying capability. As these analytical models become available, they must also be validated with experimental testing. In this experimental investigation, failure strengths of in-plane, shear-loaded bonded joints were compared with analytical predictions of the Shear-Loaded Bonded Joint (SLBJ) theory. The investigation was carried out in two phases. Phase I was conducted with a particular focus placed on the effect of bondline thickness on joint strength. Phase I specimens were fabricated using E-glass/epoxy cloth and PTM&W ES6292 two-component paste adhesive. A box beam torsion test fixture was used to apply a shear loading. Phase II was carried out to investigate changes in adhesive and adherend properties on SLBJ predictions. Phase II specimens were fabricated using aluminum and carbon adherends with Loctite and Hysol EA9360 paste adhesives. Several joggle (production-style) joints were tested to investigate the effects of joggle adherend on the strength of the adhesive joint. Furthermore, a failure analysis was conducted to study the failure mechanism of these joints. Experimental data and SLBJ predictions indicated a decrease in strength as the bondline thickness was increased. SLBJ predictions for thin bondlines were comparable with experimental data, but for thick bondlines, the SLBJ predictions were lower than the experimental data. Experimental data in this investigation revealed the significance of adhesive characterization and the adhesive joint characterization. When predicting failure of the joint, one must pay attention to the failure mode because it largely contributes to the joint performance. Because SLBJ predictions were based on the adhesive plastic strain, assuming linear elastic behavior of the adherend, the validity of these predictions were limited to the joints with adhesive or cohesive failure with minimal nonlinearity of adherend materials. When these conditions were met, the SLBJ model showed good correlation with the experimental results.

17. Key Words	18. Distribution Statement
Adhesive characterization, Stress analysis, Box beam test, Lap shear	This document is available to the public through the National Technical Information Service (NTIS), Springfield, Virginia 22161.

19. Security Classif. (of this report)	20. Security Classif. (of this page)	21. No. of Pages	22. Price
Unclassified	Unclassified	67	

ACKNOWLEDGEMENT

The authors would like to acknowledge the guidance and support of Mr. Peter Shyprykevich and Dr. Larry Ilcewicz of the Federal Aviation Administration and Dr. Keith Kedward at the University of California, Santa Barbara. The authors thank Cessna Aircraft Company of Wichita, Kansas, and Cirrus Design Corporation of Duluth, Minnesota, for supplying adhesive.

TABLE OF CONTENTS

LIST OF FIGURES

LIST OF TABLES

EXECUTIVE SUMMARY

The growing applications of adhesive bonding in aircraft structures require that more emphasis be placed on analytical models to predict failure and load carrying capability. As these analytical models become available, they must also be validated with experimental testing. In this experimental investigation, failure strengths of in-plane, shear-loaded bonded joints were compared with analytical predictions of the Shear-Loaded Bonded Joint (SLBJ) theory. The investigation was carried out in two phases. Phase I was conducted with a particular focus placed on the effect of bondline thickness on joint strength. Phase I specimens were fabricated using E-glass/epoxy cloth and PTM&W ES6292 two-component paste adhesive. A box beam torsion test fixture was used to apply a shear loading. Phase II was carried out to investigate changes in adhesive and adherend properties on SLBJ predictions. Phase II specimens were fabricated using aluminum and carbon adherends with Loctite and Hysol EA9360 paste adhesives. Several joggle (production-style) joints were tested to investigate the effects of joggle adherend on the strength of the adhesive joint. A failure analysis was conducted to study the failure mechanism of these joints. Experimental data and SLBJ predictions indicated a decrease in strength as the bondline thickness was increased. SLBJ predictions for thin bondlines were comparable with experimental data, but for thick bondlines, the SLBJ predictions were lower than the experimental data. Experimental data in this investigation revealed the significance of adhesive characterization and the adhesive joint characterization. When predicting failure of the joint, one must pay attention to the failure mode because it largely contributes to the joint performance. Because SLBJ predictions were based on the adhesive plastic strain, assuming linear elastic behavior of the adherend, the validity of these predictions were limited to the joints with adhesive or cohesive failure with minimal nonlinearity of adherend materials. When these conditions were met, the SLBJ model showed good correlation with the experimental results.

1. INTRODUCTION.

1.1 OBJECTIVES.

The growing applications of adhesive-bonded structures require validation of joint strength analytically and experimentally. Stress analysis of joints requires experimentally validated analytical models that can predict the elastic limit and ultimate joint strength. In this investigation, adhesive joint characterization was advanced from specimen level to subcomponent level testing. In addition, the strength of in-plane, shear-loaded bonded joints was compared with analytical predictions using the Shear-Loaded Bonded Joint (SLBJ) theory [1]. The investigation was carried out in two phases. Phase I was conducted with particular focus on the effect of bondline thickness on joint strength. Phase I specimens were fabricated using E-glass/epoxy cloth and PTM&W ES6292 two-component paste adhesive. Phase II was carried out to investigate changes in adhesive and adherend properties on SLBJ predictions. Phase II specimens were fabricated using aluminum and carbon adherends with Loctite[1] and Hysol EA9390 paste adhesives. Joggle joints are commonly exploited in the production of airframes with adhesive joints. This issue was addressed by comparing experimental data of joggle (production-style) joints with flat joints.

1.2 BACKGROUND AND OVERVIEW OF THE RESEARCH.

The application of composite materials in airframe structures, especially for small aircraft (figure 1-1), is growing. These composite components use primarily bonded construction for both improved structural efficiency and reduced manufacturing cost. This practice was exemplified in the activities of the NASA Langley Advanced General Aviation Transport Experiments (AGATE) Integrated Design and Manufacturing (ID&M) consortium for which the Federal Aviation Administration (FAA) provide technical support, together with various members of the small aircraft manufacturing community currently developing specific applications of composite construction of new aircraft. These aircraft use bonded construction in both primary and secondary structures.

Various certification-related issues arise in the application of adhesive joining. For small manufacturers, there is a trend toward the use of unusually large bond-layer thicknesses beyond the range for which structural performance data are available. There is a general lack of agreement on stress analysis methods and failure criteria for the design of adhesive joints. Limited structural data has been released, which allows for some validation of the modeling effort to be substantiated, although a thorough experimental validation has not been initiated. The box beam torsion lap shear test program was designed to support the modeling efforts of adhesive joints. In addition, this investigation provides information regarding structural performance of several paste adhesives in a subcomponent level. This FAA-funded research was a collaborative effort between Wichita State University and Purdue University with the support of several industry partners. Lancair Aircraft of Bend, Oregon, provided guidance during modeling and the specimen design process. Cessna Aircraft of Wichita, Kansas, and Cirrus Design of Duluth, Minnesota, provided some of the materials.

[1] Cessna proprietary two-component paste adhesive manufactured by Loctite Aerospace.

FIGURE 1-1. GENERAL AVIATION AIRCRAFT USING BONDLINES IN PRIMARY AND SECONDARY STRUCTURES

For SLBJ prediction, the experimentally measured constitutive behavior of adhesive (by ASTM D 5656) was modeled by a two-parameter exponential fitting curve. Then, failure of in-plane shear-loaded bonded joints was predicted by a shear lag-based theoretical model. This model accounts for the development of large plastic strains in the adhesive prior to failure. These analytically predicted values were then compared with experimental data using lap shear box beam torsion testing.

2. SHEAR-LOADED BONDED JOINT FAILURE PREDICTION.

The failure of in-plane, shear-loaded bonded joints is predicted using a shear lag-based theoretical model. This model accounts for the development of large plastic strains in the adhesive prior to failure by modeling experimentally obtained shear stress-strain curves using two-parameter exponential fitting curves. Failure of the adhesive is predicted by solving the governing differential equations using the Runge-Kutta method and the failure strain as measured by ASTM D 5656 and simulated by the curve fit as the initial conditions. Therefore, for this failure prediction analysis to be successful, a series of ASTM D 5656 tests must be performed for bondline thicknesses of interest. A procedure for describing adhesive plasticity in the form of a nonlinear constitutive relationship and the calculation of joint failure are detailed in this section of the report.

2.1 ADHESIVE CONSTITUTIVE BEHAVIOR.

The shear stress-strain behavior for a ductile adhesive can be modeled by a two-parameter exponential fitting curve [2]:

$$\tau_a = (G_a - kB_1)\gamma_a + B_1(1 - e^{-k\gamma_a}) \tag{2-1}$$

In this equation, k and B_1 are fitting parameters chosen in order to match the fitting curve to experimentally measured shear stress-strain data, and G_a is the elastic shear modulus.

The experimentally measured constitutive behavior (by ASTM D 5656) of three different paste adhesives is plotted in figures 2-1 through 2-3. These adhesives are PTM&W ES6292, Hysol EA9360, and a Cessna Aircraft Company proprietary Loctite formulation. Based on these figures, two general observations are noted: (1) the ultimate strain decreases with increasing adhesive bondline thickness and (2) the final stress, τ_{final}, at the failure strain can be less than the ultimate strength τ_{ult}, such that the stress versus strain curve ends with a negative slope. For Hysol EA9360 and PTM&W ES6292 adhesives, the ultimate strength decreased with increasing bondline thickness (see figures 2-1 and 2-2), while the Loctite adhesive ultimate strength increased (see figure 2-3). Fitting curves to the adhesive shear stress-strain data should reflect the aforementioned attributes, and the shear modulus G_a should be carefully chosen so as to effectively represent the entire elastic range, e.g., $0 < \gamma_a < 0.03$, for these adhesives, and not just the initial slope of the adhesive exactly at $\gamma_a = 0$.

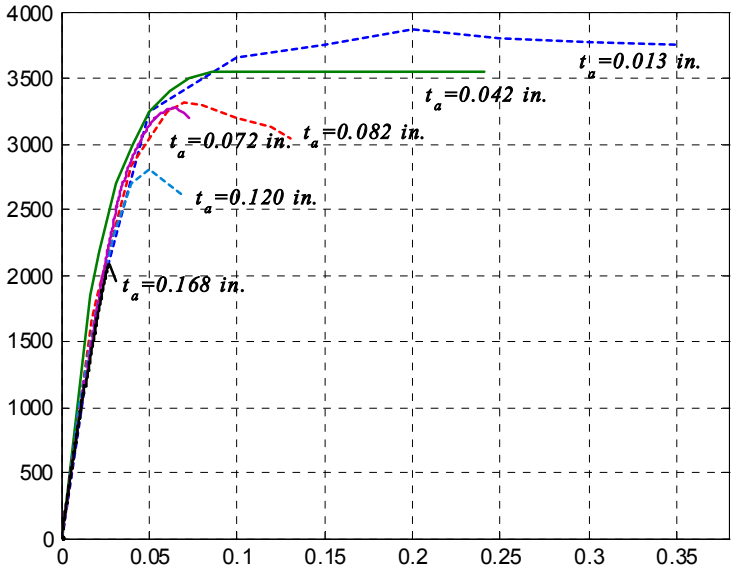

FIGURE 2-1. SHEAR STRESS-STRAIN DATA FOR PTM&W ES6292

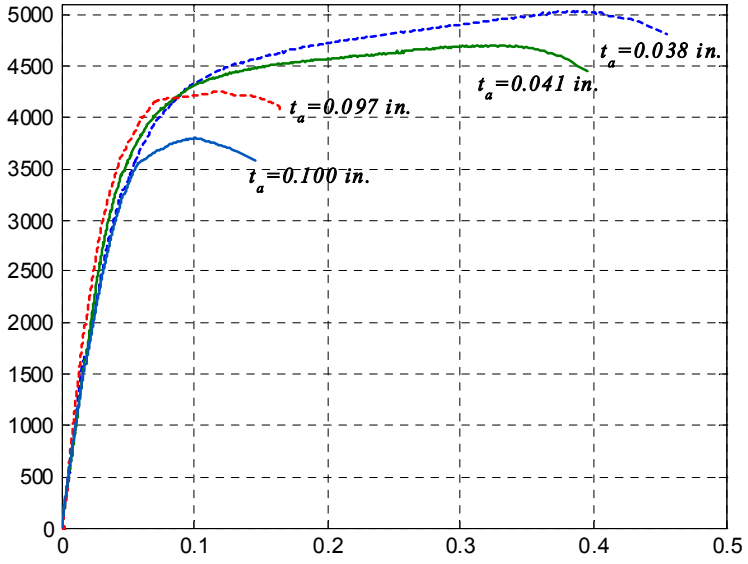

FIGURE 2-2. SHEAR STRESS-STRAIN DATA FOR HYSOL EA9360

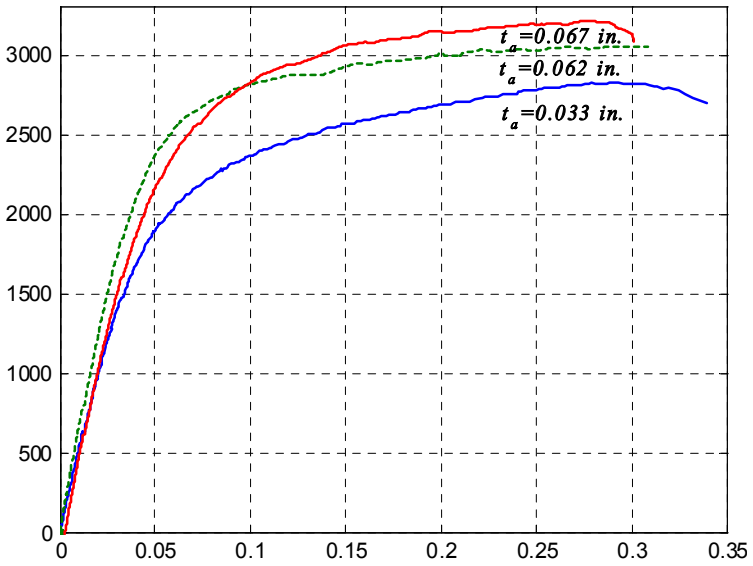

FIGURE 2-3. SHEAR STRESS-STRAIN DATA FOR LOCTITE

The parameters, k and B_1, are chosen based on the following conditions: (a) the final stress at ultimate strain γ_a^{ult} should equal the average between the ultimate and final stress (τ_{ult} and τ_{final}), and (b) the area of the fitting curve should match the area of the experimental data. Condition (a) can be expressed using equation 2-1 as follows:

$$(G_a - kB_1)\gamma_a^{ult} + B_1(1 - e^{-k\gamma_a^{ult}}) = \frac{1}{2}(\tau_{ult} + \tau_{final}) \tag{2-2}$$

The manipulation of equation 2-2 yields an expression relating B_1 as a function of k:

$$B_1 = \frac{0.5(\tau_{ult} + \tau_{final}) - G_a\gamma_a^{ult}}{1 - k\gamma_a^{ult} - e^{-k\gamma_a^{ult}}} \tag{2-3}$$

In order to satisfy condition (b), the integration of equation 2-1 with respect to γ_a between the limits 0 to γ_a^{ult} should be same as the area under the experimentally measured stress-strain curve:

$$\frac{1}{2}(G_a - kB_1)(\gamma_a^{ult})^2 + B_1[\gamma_a^{ult} + \frac{1}{k}(e^{-k\gamma_a^{ult}} - 1)] = W_{TOT} \tag{2-4}$$

where W_{TOT} is the total work per unit volume of the adhesive and is equivalent to the area under the experimental data curve.

Finally, B_1 from equation 2-3 can be inserted into equation 2-4 resulting in a transcendental equation for k, which must be solved numerically, e.g., using bisection or Newton methods. The

parameters k and B_1 were determined for the three adhesive systems shown in figures 2-1 to 2-3, and are summarized in table 2-1 for each bondline thickness. Using these values, equation 2-1 is plotted and compared to the data in figures 2-4 through 2-13.

TABLE 2-1. ADHESIVE CONSTITUTIVE MODEL FITTING PARAMETERS k AND B_1

Adhesive	t_a (in.)	k	B_1 (psi)	γ_a^{ult}
PTM&W ES6292 $G_a = 0.134$ Msi	0.013	36.4	3679	0.350
	0.042	35.6	3803	0.241
	0.072	33.4	4301	0.073
	0.082	40.0	3746	0.130
	0.120	36.8	4065	0.070
	0.168	60.6	2094	0.031
Hysol EA9360 $G_a = 0.124$ Msi	0.039*	26.2	4741	0.425
	0.098*	23.5	5759	0.155
Loctite $G_a = 0.070$ Msi	0.033	27.3	2544	0.334
	0.065*	21.5	3288	0.305

*Average thickness

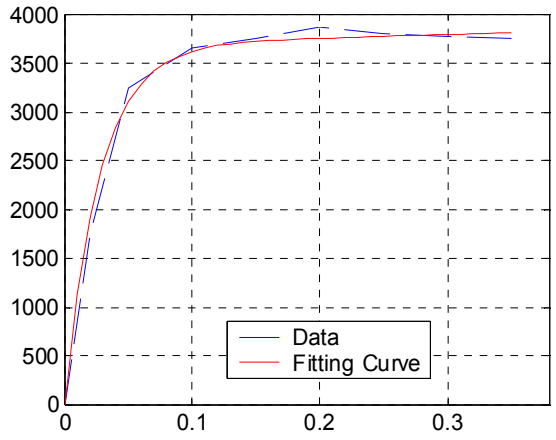

FIGURE 2-4. FIT TO DATA FOR PTM&W ES6292, $t_a = 0.013$ in.

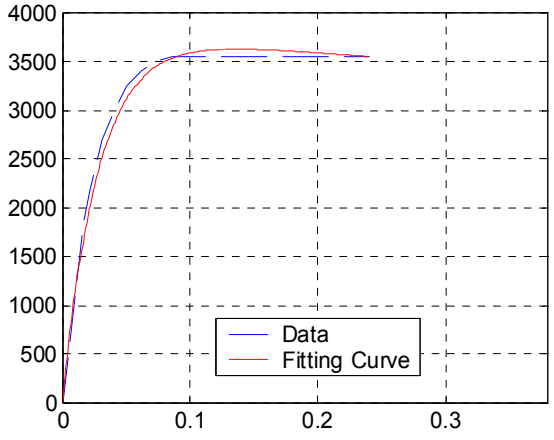

FIGURE 2-5. FIT TO DATA FOR PTM&W ES6292, $t_a = 0.042$ in.

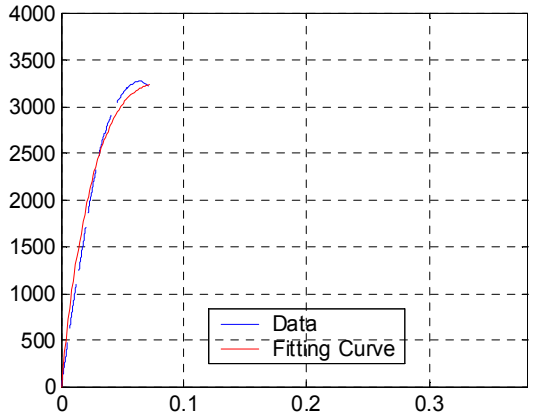

FIGURE 2-6. FIT TO DATA FOR PTM&W ES6292, $t_a = 0.072$ in.

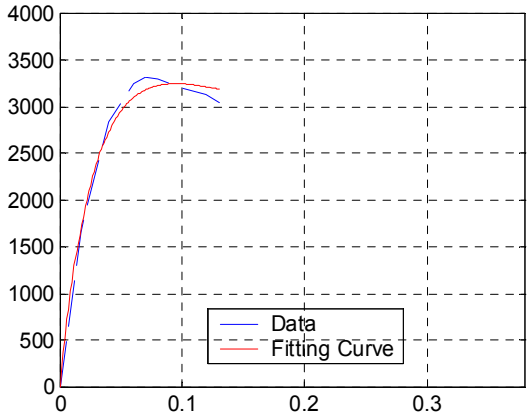

FIGURE 2-7. FIT TO DATA FOR PTM&W ES6292, $t_a = 0.082$ in.

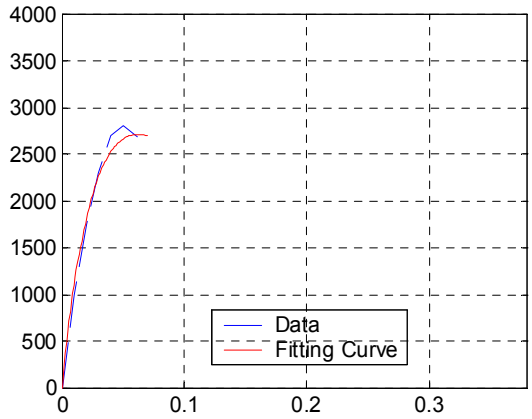

FIGURE 2-8. FIT TO DATA FOR PTM&W ES6292, $t_a = 0.120$ in.

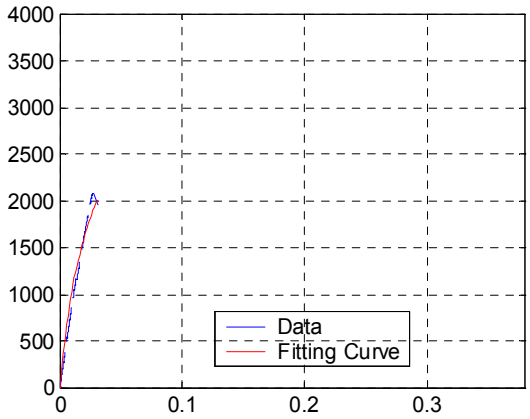

FIGURE 2-9. FIT TO DATA FOR PTM&W ES6292, $t_a = 0.168$ in.

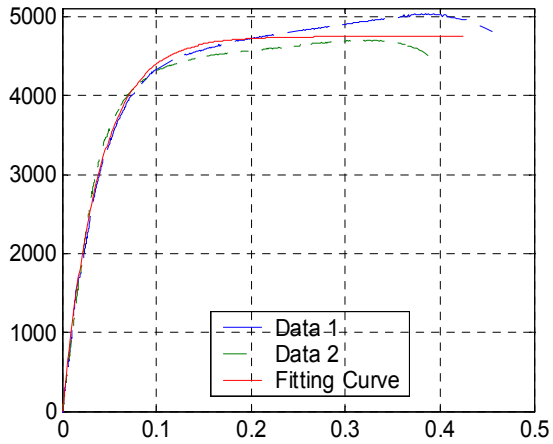

FIGURE 2-10. FIT TO DATA FOR HYSOL EA9360, $t_a = 0.039$ in.

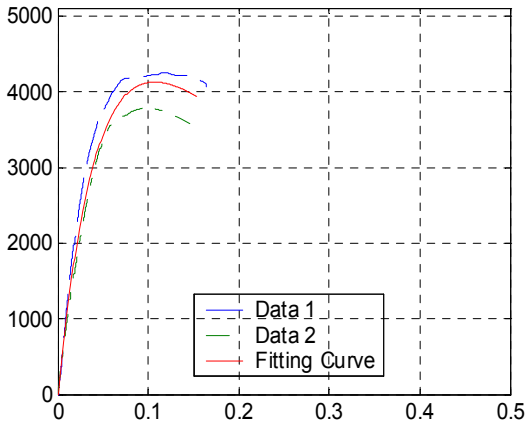

FIGURE 2-11. FIT TO DATA FOR HYSOL EA9360, $t_a = 0.098$ in.

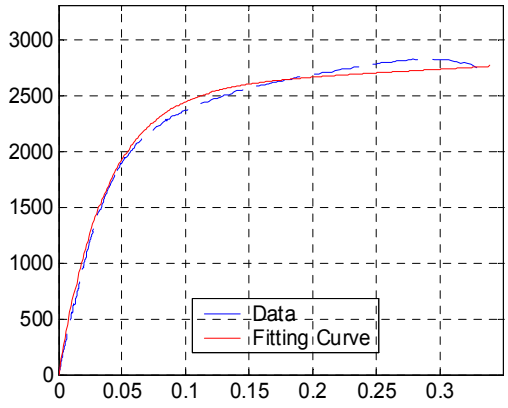

FIGURE 2-12. FIT TO DATA FOR LOCTITE, $t_a = 0.033$ in.

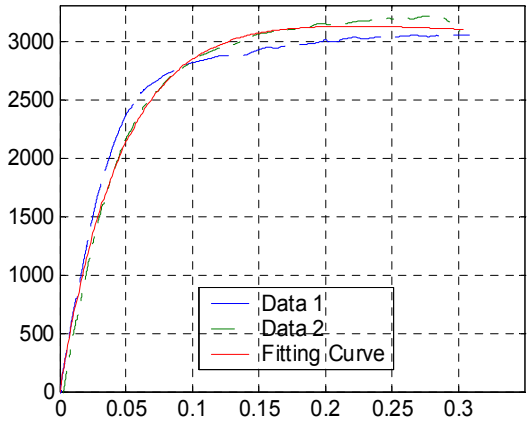

FIGURE 2-13. FIT TO DATA FOR LOCTITE, $t_a = 0.065$ in.

2.2 GOVERNING EQUATION.

The single lap joint shown in figure 2-14 is loaded by in-plane shear stress. The differential element in this figure shows the in-plane shear stress acting on the inner and outer adherends, τ^i_{xy} and τ^o_{xy}, as well as two components of the adhesive shear stress, τ^a_{xz} and τ^a_{yz}. The following conditions have been assumed:

- constant bond and adherend thickness
- uniform shear strain through the adhesive thickness
- adherends carry only in-plane stresses
- adhesive carries only out-of-plane shear stresses

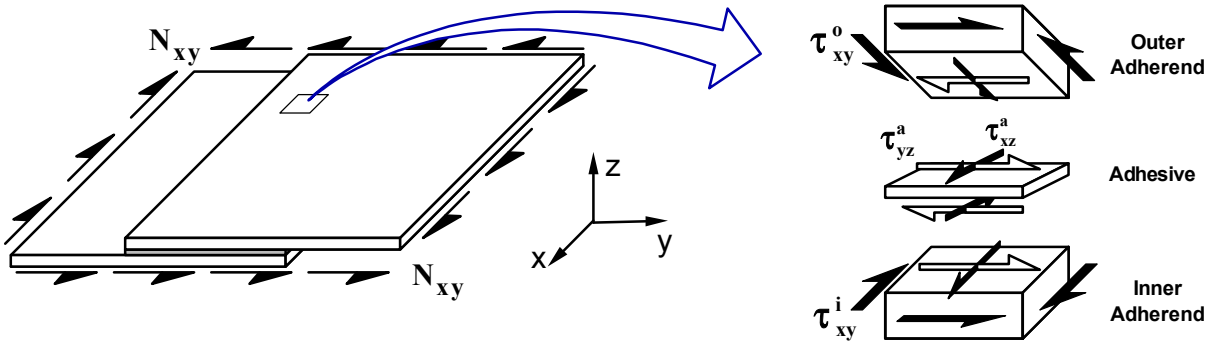

FIGURE 2-14. LAP JOINT TRANSFERRING SHEAR STRESS RESULTANT N_{xy} AND DIFFERENTIAL ELEMENT SHOWING ADHEREND AND ADHESIVE STRESSES

In figure 2-14, the applied in-plane shear stress resultant N_{xy} is continuous through the overlap region and, at any point, must equal the sum of the product of each adherend shear stress with its respective thickness t_i and t_o:

$$N_{xy} = \tau_{xy}^{i} t_i + \tau_{xy}^{o} t_o \tag{2-5}$$

The adhesive shear strains are written based on the assumption of a uniform distribution through the thickness of the adhesive as follows:

$$\gamma_{xz}^{a} = \frac{1}{t_a}(u_o - u_i) \quad \text{and} \quad \gamma_{yz}^{a} = \frac{1}{t_a}(v_o - v_i) \tag{2-6) and (2-7}$$

where t_a is the thickness of the adhesive and *u* and *v* are the in-plane deformations in each adherend. Differentiating equation 2-7 with respect to *x* and equation 2-6 with respect to *y* and adding the two resulting equations, results in the following:

$$\frac{\partial \gamma_{xz}^{a}}{\partial y} + \frac{\partial \gamma_{yz}^{a}}{\partial x} = \frac{1}{t_a}(\gamma_{xy}^{o} - \gamma_{xy}^{i}) = \frac{1}{t_a}\left(\frac{\tau_{xy}^{o}}{G_o} - \frac{\tau_{xy}^{i}}{G_i}\right) \tag{2.8}$$

From equation 2-5, shear stress in the inner adherend can be written as follows:

$$\tau_{xy}^{i} = \frac{N_{xy} - \tau_{xy}^{o} t_o}{t_i} \tag{2-9}$$

Substituting equation 2-9 into equation 2-8 yields

$$\frac{\partial \gamma_{xz}^{a}}{\partial y} + \frac{\partial \gamma_{yz}^{a}}{\partial x} = \frac{t_o}{t_a}\left(\frac{\tau_{xy}^{o}}{G_o t_o} + \frac{\tau_{xy}^{o}}{G_i t_i}\right) - \frac{N_{xy}}{t_a G_i t_i} \tag{2-10}$$

Force equilibrium performed on a differential element of the outer adherend, shown in figure 2-15, results in relationships between the adhesive stress components and the outer adherend shear stress:

$$\tau_{xz}^{a} = t_o \frac{\partial \tau_{xy}^{o}}{\partial y} \quad \text{and} \quad \tau_{yz}^{a} = t_o \frac{\partial \tau_{xy}^{o}}{\partial x} \tag{2-11) and (2-12}$$

Summing the derivative of equation 2-10 with respect to *x* with the derivative of equation 2-10 with respect to *y* and simplifying using equations 2-11 and 2-12, results in the general two-dimensional governing equation for adhesive shear strain:

$$\frac{\partial^2 \gamma_{xz}^{a}}{\partial y^2} + \frac{\partial^2 \gamma_{xz}^{a}}{\partial x \partial y} + \frac{\partial^2 \gamma_{yz}^{a}}{\partial x^2} + \frac{\partial^2 \gamma_{yz}^{a}}{\partial x \partial y} = \frac{1}{t_a}\left(\frac{1}{G_o t_o} + \frac{1}{G_i t_i}\right)(\tau_{yz}^{a} + \tau_{xz}^{a}) \tag{2-13}$$

For the one-dimensional joint shown in figure 2-16, all partial derivatives with respect to *x* would be zero. This simplification is applicable to loading that is smoothly varying or independent of the *x* axis [3]. By incorporating the adhesive constitutive behavior from equation 2-1, the governing equation for this problem is derived as follows:

$$\frac{d^2\gamma_{xz}^a}{dy^2} = \lambda^2[(1-\frac{kB_1}{G_a})\gamma_{xz}^a + \frac{B_1}{G_a}(1-e^{-k\gamma_{xz}^a})] \tag{2-14}$$

$$\text{where } \lambda^2 = \frac{G_a}{t_a}(\frac{1}{G_o t_o} + \frac{1}{G_i t_i}) \tag{2-15}$$

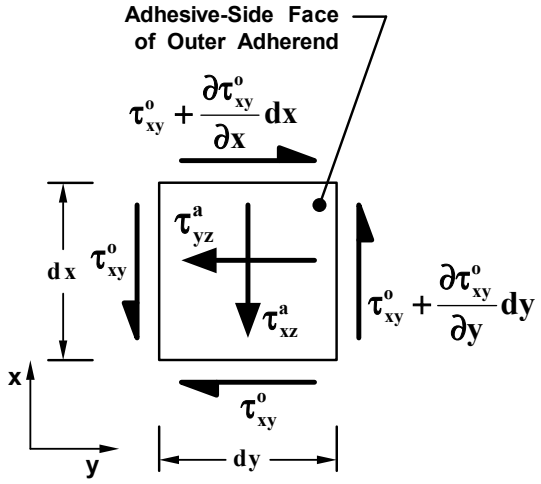

FIGURE 2-15. ADHESIVE AND ADHEREND STRESSES ACTING ON ELEMENT OF OUTER ADHEREND

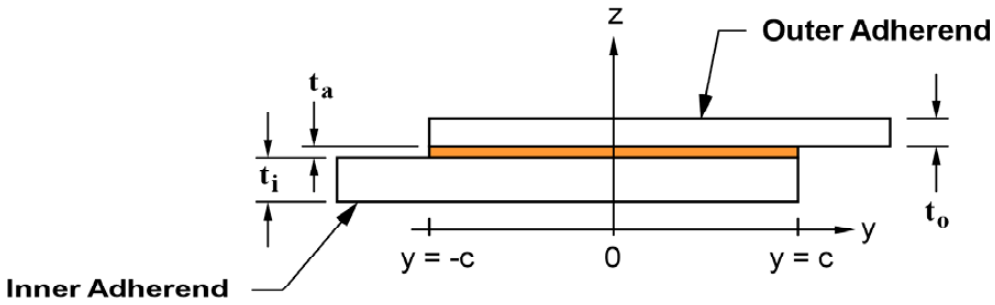

FIGURE 2-16. SINGLE LAP OR SYMMETRIC DOUBLE LAP JOINT

Since this governing equation cannot be solved in closed form, the numerical Runge-Kutta fourth order with shooting method is applied to obtain a solution. Boundary conditions for this problem are defined as

$$\text{at } y = -c,\ \tau_{xy}^{o} = 0 \tag{2-16}$$

$$\text{at } y = c,\ \tau_{xy}^{o} = \frac{N_{xy}}{t_o} \tag{2-17}$$

Note, however, that equation 2-14 is in adhesive strain, so these boundary conditions need to be transformed using the one-dimensional form of equation 2-10 to be consistent with solving equation 2-14. This results in the following strain gradient boundary conditions:

$$\text{at } y = -c,\ \left.\frac{d\gamma_{xz}^{a}}{dy}\right|_{y=-c} = -\frac{N_{xy}}{t_a G_i t_i} \tag{2-18}$$

$$\text{at } y = c,\ \left.\frac{d\gamma_{xz}^{a}}{dy}\right|_{y=c} = \frac{N_{xy}}{t_a G_o t_o} \tag{2-19}$$

The Runge-Kutta method requires two initial conditions rather than two boundary conditions. These can be applied at either y = -c or at y = c. Thus, to predict failure, first the strain at either end of the joint is set as the failure strain γ_a^{ult} (e.g., at y = -c). Then for a given guess of the failure load N_{xy}, the strain gradient boundary condition calculated by equation 2-18 or 2-19 is used as the second initial condition (e.g., equation 2-18 is used to compute slope at y = -c). The numerical solution using the Runge-Kutta method reveals the predicted strain distribution along the overlap length. At the other end of the joint, opposite to the side initial conditions were applied (e.g., at y = c), the calculated strain gradient is compared with the remaining strain gradient boundary condition (e.g., equation 2-19 at y = c). If these values are not matched, an iteration on the value of load N_{xy} must be made (this affects the slope boundary conditions), and the strain distribution then is recalculated and compared against the boundary conditions. This process is repeated iteratively until both boundary conditions are satisfied.

2.3 EXAMPLE CALCULATION.

Failure prediction is demonstrated for a joint with glass/epoxy cloth adherends of lay-up $[0_4/45/-45/0_4]$, overlap length 2c = 1.0 inch, and bonded by PTM&W ES6292 adhesive. The joint parameters used in this calculation are listed in table 2-2. The elastic limit load N_{xy}^{e} can be calculated based on the assumption of elastic-to-failure adhesive stress-strain behavior [3]:

$$N_{xy}^{e} = \frac{2c\tau_{ult}\tanh\lambda c}{\lambda c} \tag{2-20}$$

N_{xy}^{e} can be considered a conservative prediction of joint failure since it does not account for any adhesive plasticity. The τ_{ult} can be selected for either the yield stress or the ultimate stress listed in table 2-2.

TABLE 2-2. EXAMPLE CALCULATION JOINT PARAMETERS

Joint Parameters	Value
t_o (in.)	0.098
t_i (in.)	0.098
t_a (in.)	0.013
G_o (Msi)	0.843
G_i (Msi)	0.843
G_a (Msi)	0.112
τ_{ult} (psi)	3875

When conducting the nonlinear failure prediction (using equation 2-14), the applied load corresponding to the ultimate failure strain γ_a^{ult} in the adhesive is determined by the previously described procedure. The failure load is N_{xy}^{f}. The profiles of adhesive shear strain and stress at failure load are plotted in figure 2-17. Note that the adhesive shear stress profile shows significant plasticity development at the ends of the overlap. For this case study example, the elastic limit (equation 2-20) and the failure limit (equation 2-14) loads are predicted to be $N_{xy}^{e} = 490$ lbf/in. and $N_{xy}^{f} = 2281$ lbf/in., respectively. Comparing the loads in this case example shows that the elastic limit is conservative by a factor of over four times.

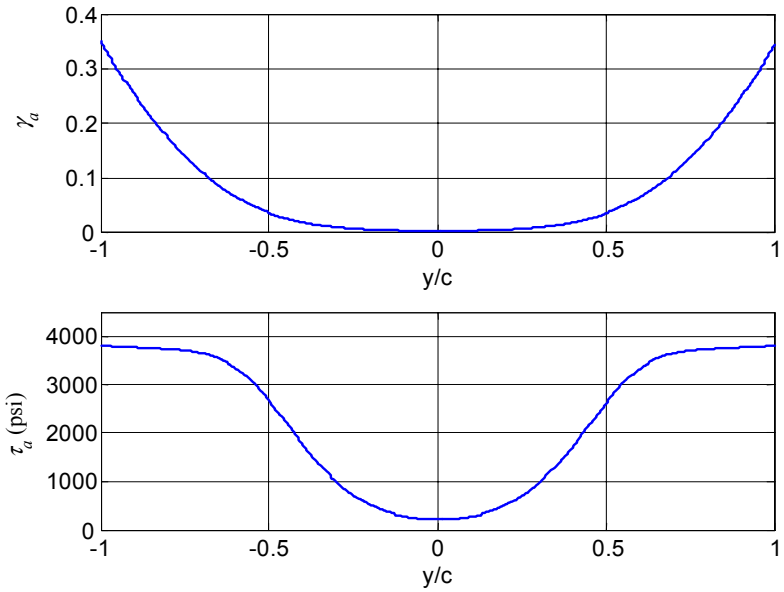

FIGURE 2-17. ADHESIVE SHEAR STRAIN AND STRESS AT FAILURE LOAD FOR JOINT WITH $t_a = 0.013$ in.

2.4 FINITE ELEMENT ANALYSIS VALIDATION.

Finite Element Analysis (FEA) was used to verify the theoretical predictions of the shear stress distribution in a single lap joint. In order to model a state of pure in-plane applied shear loading using two-dimensional FEA, axisymmetric elements were used to model two thin-walled cylinders with large radius ($r = 80$ inches) bonded to each other. The cross section of this joined cylinder represents the single lap joint described in figure 2-16. A rotation was applied at one boundary of the cylinder, and the other end was fixed against rotation, thereby producing a state of in-plane shear. This approach permitted the use of a two-dimensional axisymmetric model (with nonaxisymmetric loading) instead of a fully three-dimensional model. Two-dimensional axisymmetric quadratic eight-node elements CGAX8R in ABAQUS [4] were used in this analysis, which incorporated the nonlinear adhesive behavior shown in figure 2-4.

Failure of the joint is believed to occur when the strain at any integration point in the adhesive elements reaches the ultimate shear strain, γ_a^{ult}. As shown in figure 2-18, the peak predicted plastic strain was localized at the interface corner between the adhesive and adherend, at the end of the overlap (at $y = c$) along path 3, and similarly at the opposite end (at $y = -c$) along path 1. Paths 1 and 3 pass through the integration points in the adhesive elements located closest to the adhesive-to-adherend interface (roughly 0.0007 inch for this model). Path 2 passes through the adhesive centerline. If the plastic strain at the integration point nearest this interface corner reaches the failure strain of the adhesive, the analysis is terminated, and the corresponding load is interpreted as the failure load.

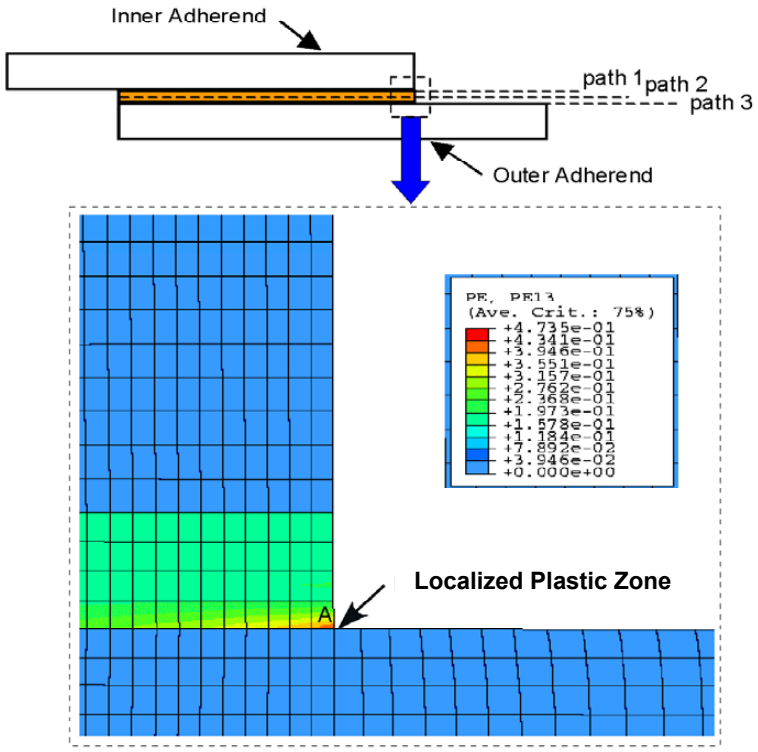

FIGURE 2-18. LOCALIZED PLASTIC STRAIN PREDICTED BY FEA FOR JOINT WITH $t_a = 0.013$ in.

The strain predicted by FEA for a joint with $t_a = 0.013$ in. is plotted in figure 2-19 along the three paths indicated in figure 2-18. The divergence of results plotted along these paths indicates that there exists a gradient in strain through the adhesive thickness near the ends of the overlap. The theoretical model prediction, which assumes uniform strain through the adhesive thickness, is also shown in figure 2-19. Note that in figure 2-19, the plotted strain component is plastic strain and not total strain. For this case study, the applied load associated with failure is predicted by the FEA to be 2281 lbf/in. and by the theoretical model to be 2400 lbf/in. (5.2% above FEA).

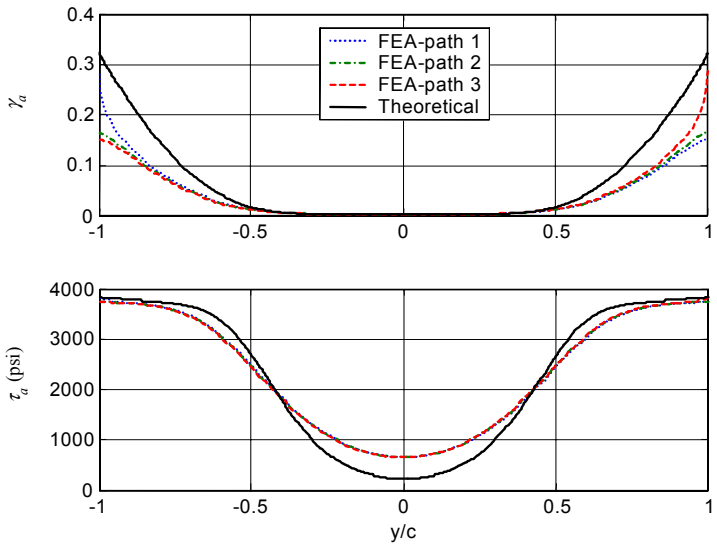

FIGURE 2-19. SHEAR STRAIN AND SHEAR STRESS AT FAILURE LOAD FOR JOINT WITH $t_a = 0.013$ in.

Two additional thickness cases were studied and compared with FEA predictions. The details of these calculations can be found in reference 1 and are summarized in table 2-3. The FEA results for these thicker cases show that the strain localization observed in figures 2-18 and 2-19 is more severe for increasing bondline thickness. Due to this localization of strain not being accounted for, the theoretical model tended to overpredict the failure load. Table 2-3 shows the percent error of the theoretical calculation relative to FEA prediction. For these case studies, the theoretical solution was found to be accurate within 23% for considerably thick adhesive bondlines (up to 0.042 inch). For more conventional thickness joints (less than 0.015 inch), the theoretical prediction is accurate to within 6% relative to FEA prediction.

TABLE 2-3. THEORETICAL MODEL AND FEA COMPARISON

t_a (in.)	Failure Limit, N_{xy}^f (lbf/in.)	
	FEA	Theoretical (% Difference)
0.013	2281	2400 (5.2)
0.042	2604	3190 (22.5)
0.082	2370	2980 (25.7)

2.5 PREDICTION OF EXPERIMENTS.

Failure load N_{xy}^{f} is predicted for the three different adhesives for in-plane shear-loaded joints having adherends, as specified in table 2-4. All joints have an overlap length of $2c$ = 0.5 in. and are configured as balanced joints, which means that the product of thickness and effective shear modulus are the same for both the outer and inner adherends. In table 2-5, predicted failure loads N_{xy}^{f} are listed for adhesive and adherend configurations and bondline thickness similar to those experimentally tested and reported in section 6 of this report. Figure 2-20 is a plot of failure load versus bondline thickness. Except for the Loctite adhesive, the predicted failure load N_{xy}^{f} was found to decrease for greater bondline thickness. The Loctite joints show a reverse trend due to the adhesive showing higher ultimate strength for a thicker bondline.

TABLE 2-4. ADHEREND PROPERTIES

Material	Thickness (in.)	Effective Shear Modulus (Msi)
Glass/Epoxy	0.098	0.843
Carbon/Epoxy	0.090	1.373
Aluminum (2024 T3)	0.050	4.060

TABLE 2-5. FAILURE LOAD PREDICTION

Adhesive	t_a (in.)	Adherend	Predicted N_{xy}^{f} (lbf/in.)
PTM&W ES6292	0.013	Glass/Epoxy	1870
	0.042		1800
	0.072		1510
	0.082		1615
	0.120		1350
	0.168		930
Hysol EA9360	0.039	Carbon/Epoxy	2380
	0.098		2010
Loctite	0.033	Aluminum	1380
	0.065		1555

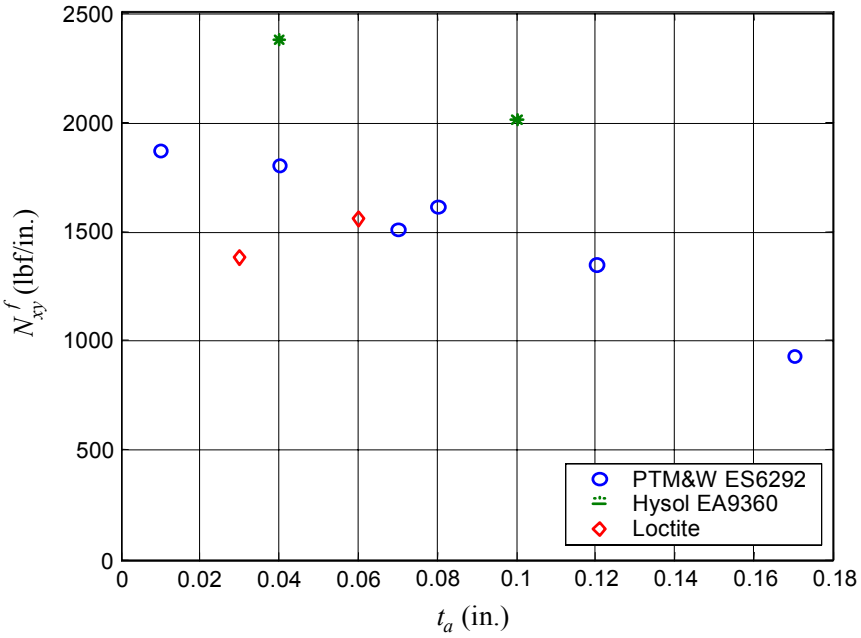

FIGURE 2-20. FAILURE LOAD PREDICTION VERSUS BONDLINE THICKNESS

3. BOX BEAM TORSION LAP SHEAR TESTING.

3.1 MATERIALS.

General aviation (GA) companies and officials from the FAA were consulted during the materials selection process. Because this program was motivated by joints found in GA aircraft, initial specimens were constructed from adhesive and adherend materials commonly used in GA airframe applications.

Box beam torsion lap shear testing was completed in two phases. Phase I focused on comparing maximum shear flow of adhesive single lap joint and prediction of SLBJ theory. Specimens of Phase I were fabricated using Newport NB321/7781 E-glass epoxy cloth and PTM&W ES6292 two-component paste adhesive system. The ES6292 adhesive system is well characterized in reference 5 and considered as a brittle adhesive system (Shear Modulus: 0.092-0.123 Msi at room temperature dry (RTD). Figure 3-1 shows characteristic shear responses of ES6292 for bondline thickness of 0.07 and 0.17 inch. As seen in previous investigations, apparent shear strength significantly decreased as bondline thickness increased.

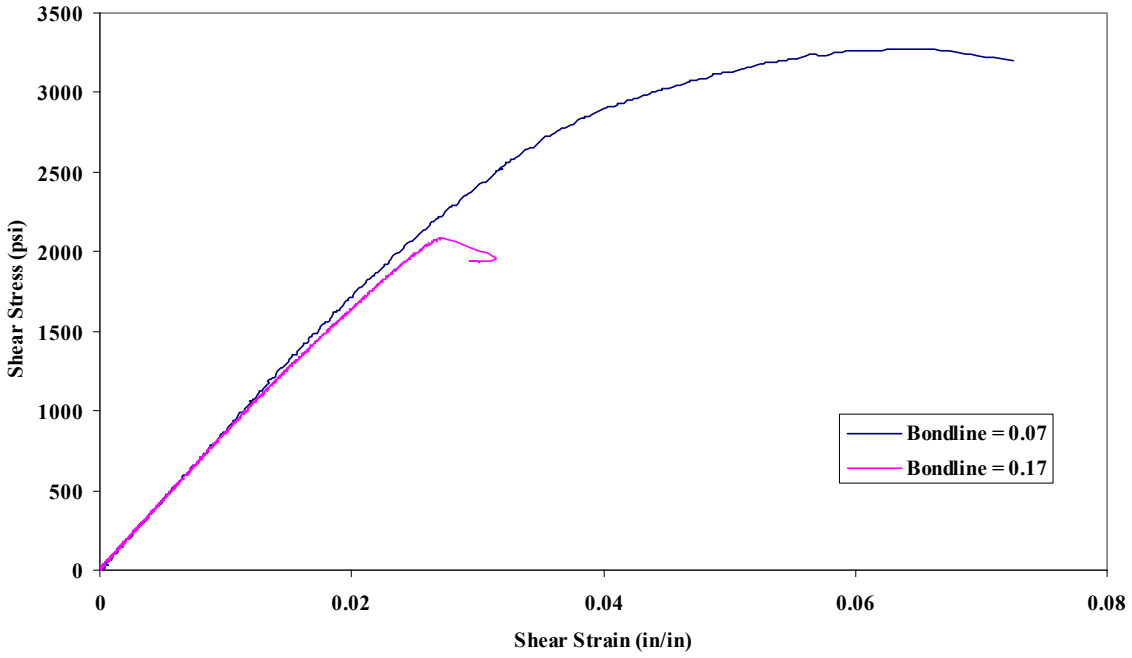

FIGURE 3-1. CHARACTERISTIC SHEAR RESPONSE OF PTM&W ES6292 UNDER RTD CONDITIONS

Each test specimen consists of two adherend laminates with a ten-ply lay-up of $[0_4/45/-45/0_4]$ to ensure a balanced and symmetric lay-up. The number of required 0° plies is driven by the thickness needed to prevent bearing failure through the bolted attachments and to resist buckling. Stiffness properties of NB321/7781 laminate with the above-mentioned ply schedule were predicted using Classical Laminate Theory (CLT) based on data obtained from the AGATE

material database [6]. The average initial in-plane shear modulus obtained, according to ASTM D 5379, for a 20-ply ($[0_4/45/-45/0_4]_s$) FG7781 fiberglass specimen was 0.84 Msi, and was comparable with CLT predictions.

Phase II of box beam testing was conducted with material that varied in both adhesive and adherend. Comparison of test results with SLBJ predictions provided information regarding capability of SLBJ theory to account for material differences. The first set of specimens in this phase was fabricated using Newport NB321/3K70P carbon cloth, which had a similar lay-up schedule as glass specimens, and a Hysol EA9360 two-component paste adhesive system. The EA9360 is a structural adhesive with high-peel strength and well characterized in reference 5. Figure 3-2 shows the characteristic shear response of EA9360 (bondline thickness = 0.10 inch) under RTD conditions. Stiffness properties of carbon cloth were calculated using similar procedures that were used for E-glass cloth, using material properties obtained from AGATE material database [7].

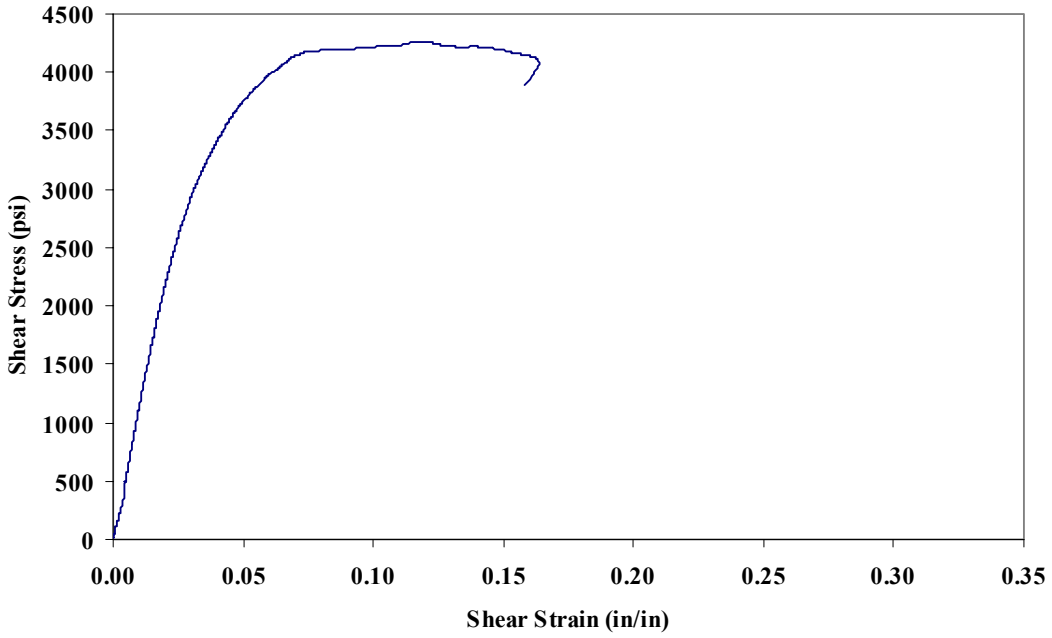

FIGURE 3-2. CHARACTERISTIC SHEAR RESPONSE OF HYSOL EA9360 UNDER RTD CONDITIONS (Bondline = 0.10 in.)

The second set of specimens in Phase II was fabricated using phosphorous-anodized and bond-primed 2024-T3 bare aluminum adherend and Loctite two-component paste adhesive. Figure 3-3 shows the characteristic shear response of Loctite under RTD conditions based on data gathered for a FAA-funded research project conducted at the National Institute for Aviation Research at Wichita State University [8].

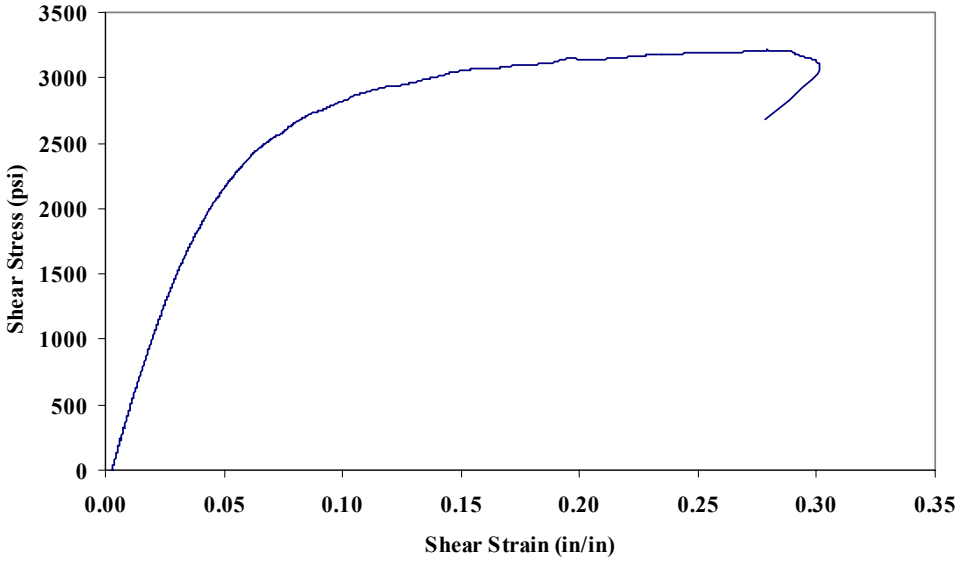

FIGURE 3-3. CHARACTERISTIC SHEAR RESPONSE OF LOCTITE ADHESIVE UNDER RTD CONDITIONS (Bondline = 0.07 in.)

To ensure that the adhesives were bonded properly to the adherend, composite subpanels were sand blasted, and aluminum subpanels were phosphorus anodized and bond primed. The ES6292 was supplied by Cirrus Design Corporation of Duluth, Minnesota, and the phosphorous-anodized and bond-primed aluminum adherend along with Loctite were supplied by Cessna Aircraft Company of Wichita, Kansas.

3.2 TEST MATRIX.

Bondline thicknesses in Phase I represent values common to GA applications. This test matrix was designed to investigate the effects of thickness on load-carrying capabilities of subcomponent level adhesively bonded joints (table 3-1). Specimens with a bondline thickness of 0.16 inch were added to this test matrix to investigate the shear flow distribution along the gage length. Therefore, a series of ±45° strain rosettes were mounted 2 inches apart along the gage length of these specimens. In addition, test results were compared with the analytical prediction of the SLBJ theory presented in section 2. The test matrix in Phase II was designed to introduce adhesive and adherend material variables to analytical predictions and compare them with test results (table 3-2). All testing was conducted at room temperature ambient conditions (RTD). In addition to flat-adherend joints, both Phase I and Phase II included joggle (production-style) joints. Joggle joints in Phase I were fabricated using ES6292 and FG7781 E-glass with bondline thicknesses of 0.05 and 0.10 inch. In Phase II, they were fabricated using EA9360 and carbon cloth with bondline thicknesses of 0.09 and 0.13 inch. Although the same two molds were used in both phases, the difference in ply thicknesses of E-glass and carbon cloths resulted in a change in bondline thickness of joggle joints.

TABLE 3-1. TEST MATRIX FOR PHASE I

Adhesive	Joint Type	Adherend	Bondline Thickness (in.)	Number of Specimens
ES6292	Flat	E-Glass	0.01	4
			0.05	4
			0.10	4
			0.16	4
			0.20	4
ES6292	Joggle	E-Glass	0.05	4
			0.10	4

TABLE 3-2. TEST MATRIX FOR PHASE II

Adhesive	Joint Type	Adherend	Bondline Thickness (in.)	Number of Specimens
EA 9360	Flat	Carbon	0.10	4
Loctite	Flat	Aluminum	0.05	2
ES6292	Flat	Fiber glass	0.10	4*
EA 9360	Joggle	Carbon	0.09	2
			0.13	2

*Test data from Phase I was used for comparison.

3.3 SPECIMEN CONFIGURATION.

Two different types of specimens were tested in a torsion-only loading configuration. Specimens in Phase I consisted of two flat-adherend laminates with a ten-ply lay-up $[0_4/45/-45/0_4]$. Initial specimens were fabricated according to the dimensions shown in drawing UCSB-BB-030 in appendix A. The larger overlap length shown here more closely represents an actual aircraft bonded structure. During calibration of the test fixture, it was found that the failure loads of these specimens were higher than the fixture capacity. In order to obtain failure of the specimen within the capacity of the fixture, overlap length was decreased to 0.5 inch. Coupon level testing conducted to characterize adhesive according to the recommendation in the ASTM D 5656 standard uses an overlap length of 0.375 inch and demonstrated satisfactory test results. Thus, a 0.5-inch overlap was considered to be sufficient for this investigation. In addition, overall length of the specimen was increased from 12 to 17.25 inches (figure 3-4) in order for the middle region of the specimen to have uniform shear flow.

The second series of specimens in Phase I had joggle joints, as shown in figure 3-5. They were fabricated with the two above-mentioned modifications to the gage section. These specimens are representative of actual production style joints. Two aluminum molds were machined to fabricate joggle joints with 0.05- and 0.10-inch bondline thicknesses for ten-ply E-glass adherends. Curvature of the joggle section was designed to minimize resin-rich areas due to bridging of the composite plies.

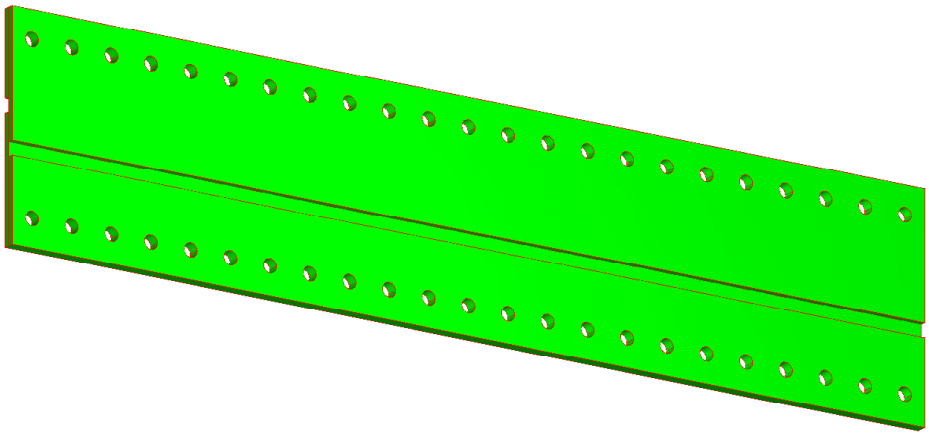

FIGURE 3-4. TEST SPECIMEN WITH TWO FLAT ADHEREND S

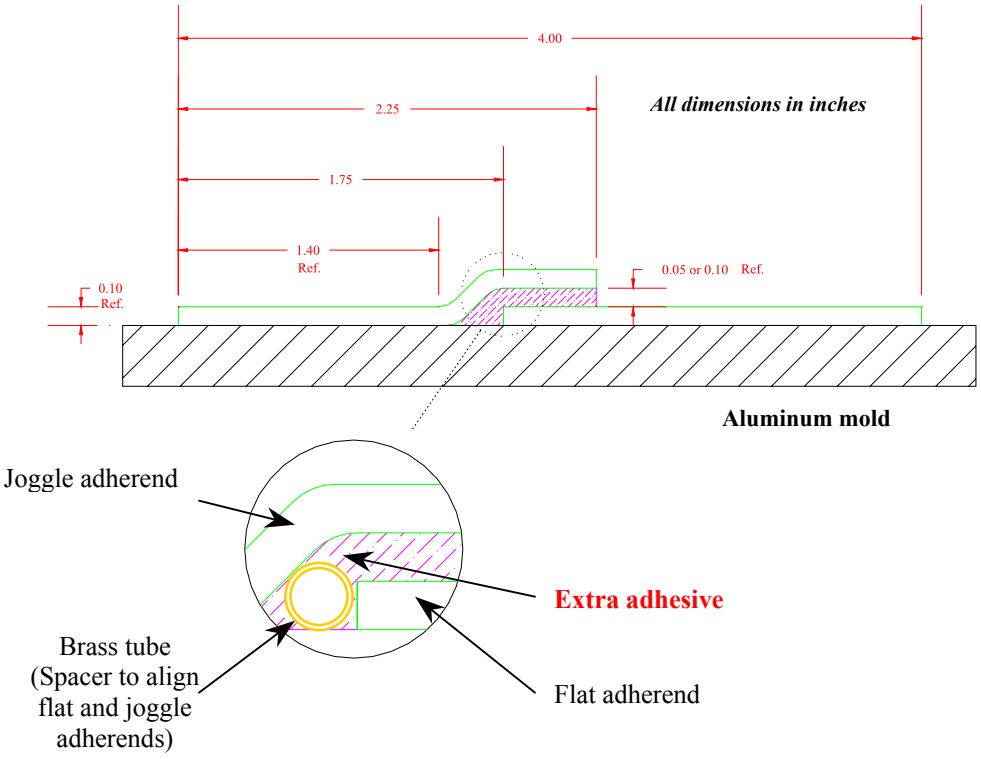

FIGURE 3-5. TEST SPECIMEN WITH JOGGLE JOINT

4. PANEL FABRICATION AND MACHINING.

4.1 ADHESIVE TEST PANEL FABRICATION.

Subpanels were grouped into sets of two, and reference points were marked so that bonded test panels would have the same reference point on both sides. Subpanel surfaces were cleaned several times with acetone and lint-free cotton towels, using a sweeping motion. This step in the process was important to ensure that the surface was adequately prepared for proper bonding of the adhesive-laminate (or aluminum) interface. Care was taken not to scratch the surface but to remove grease and other foreign substances. This procedure should be repeated at least once to produce a clean surface. Poorly cleaned surfaces increase the chance of failure in an adhesive specimen due to voids in the adhesive-laminate interface.

To achieve a constant bondline thickness, brass shims or spacers were bonded to one panel using double-sided tape (figure 4-1). Care was taken not to leave any spacers in the gage section. In a previous investigation, it was found that double-sided tape provided a more even distribution of thickness than liquid glue. After the spacers were bonded, the subpanel surface was cleaned once more with acetone.

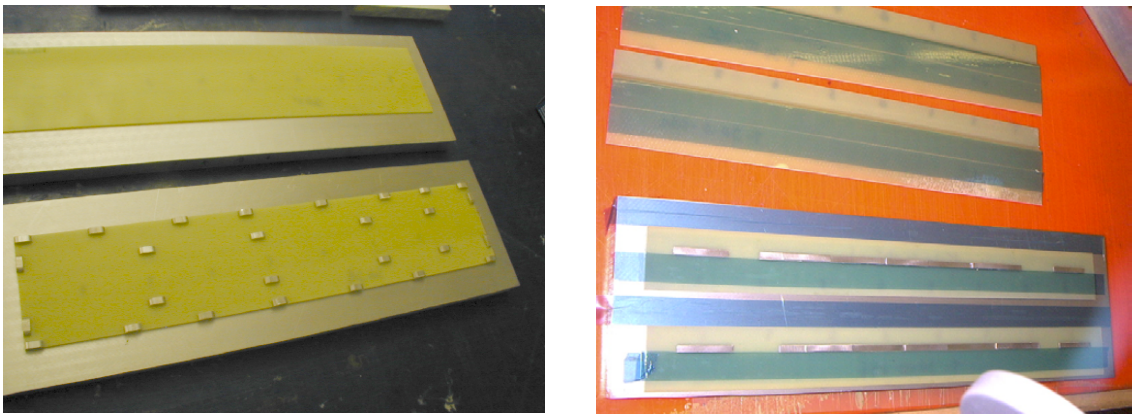

(a) (b)

FIGURE 4-1. SPACER LOCATIONS FOR (a) FLAT AND (b) JOGGLE JOINT SPECIMENS

The resin and accelerator were mixed in a cup using a prescribed mix ratio and then applied to the subpanel. Care was taken to evenly distribute the adhesive over the subpanel with the spacers and especially over the gage section (figure 4-2). A thin layer of adhesive was applied over a second subpanel in order to provide a wet surface and diminish potential voids in the adhesive-laminate interface. Subsequently, the second subpanel was tilted and gradually placed over the first subpanel to expel any trapped air.

Once the adhesive was applied, subpanels were taped with flash breaker tape to avoid any movement during the cure cycle. Joggle joint specimens were clamped, as shown in figure 4-3. Care was taken to evenly torque C-clamps to avoid uneven bondline thickness. The adhesive was cured according to the specified temperature and pressure obtained from the manufacturers data sheet. A programmable oven was used to regulate the cure process. The temperature

control thermocouple monitored the adhesive temperature. After the panels were cured, the final thickness was measured at the reference points in order to calculate the bondline thickness, which was used in two of the machining steps, discussed in the section 4.2.

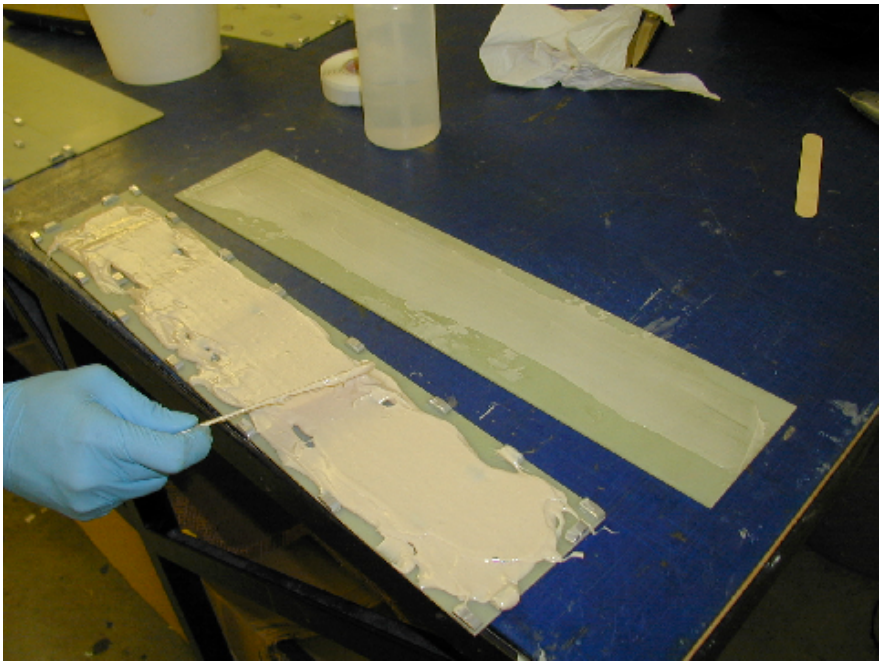

FIGURE 4-2. PASTE ADHESIVE APPLICATION FOR FLAT SPECIMENS

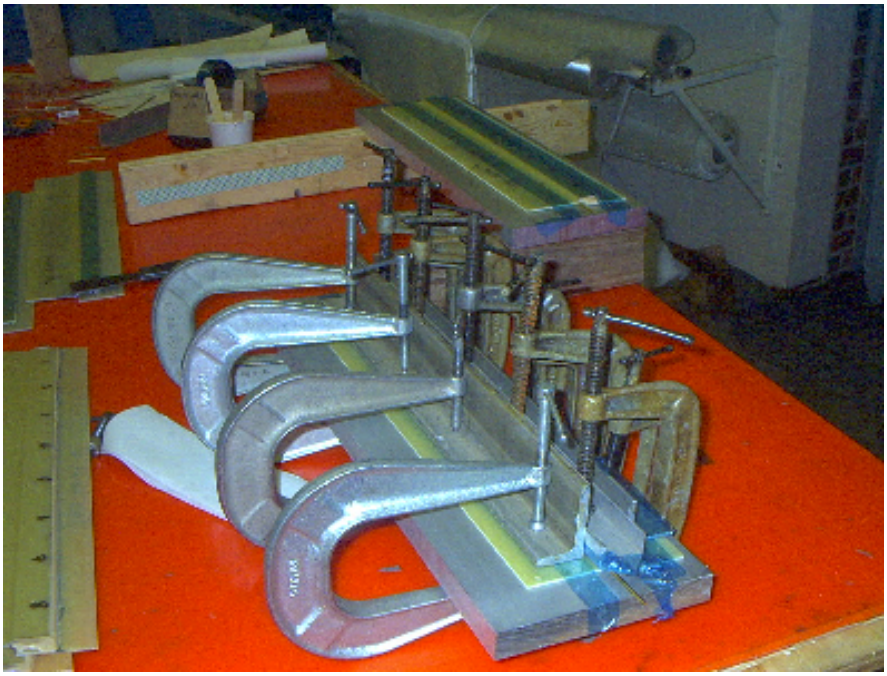

FIGURE 4-3. JOGGLE JOINT ADHESIVE PANEL FABRICATION

4.2 MACHINING OF LAP SHEAR ADHESIVE SPECIMENS.

Adhesive lap shear specimens were machined using a Bridgeport® CNC machine. Tool paths were created using MasterCam Version 7.

- Panels were rough cut with 0.025-inch extra material around using a band saw.
- Using the CNC machine, 0.25- and 0.375-inch boltholes were drilled and reamed with 0.251- and 0.378-inch reamers, respectively.
- Each specimen was machined (end milled) to the final dimensions specified.
- 0.25-inch slots were machined on each side of the specimen to obtain a 0.5-inch gage section.

CNC machining was conducted with abundant coolant to ensure that the specimens were not overheated during the process.

Following machining, specimens were named using the nomenclature shown in figure 4-4 for tracability. The first letter indicates the loading configuration. All testing in this investigation was conducted in torsion-only configuration. The second letter indicates the type of joint, i.e., flat (F) or joggle (J). Third and fourth letters indicate the adhesive and adherend material, respectively. The next three numbers represent the approximate bondline thickness in thousandth of an inch. The final number represents the replica number with the same parameters given by previous letters and numbers.

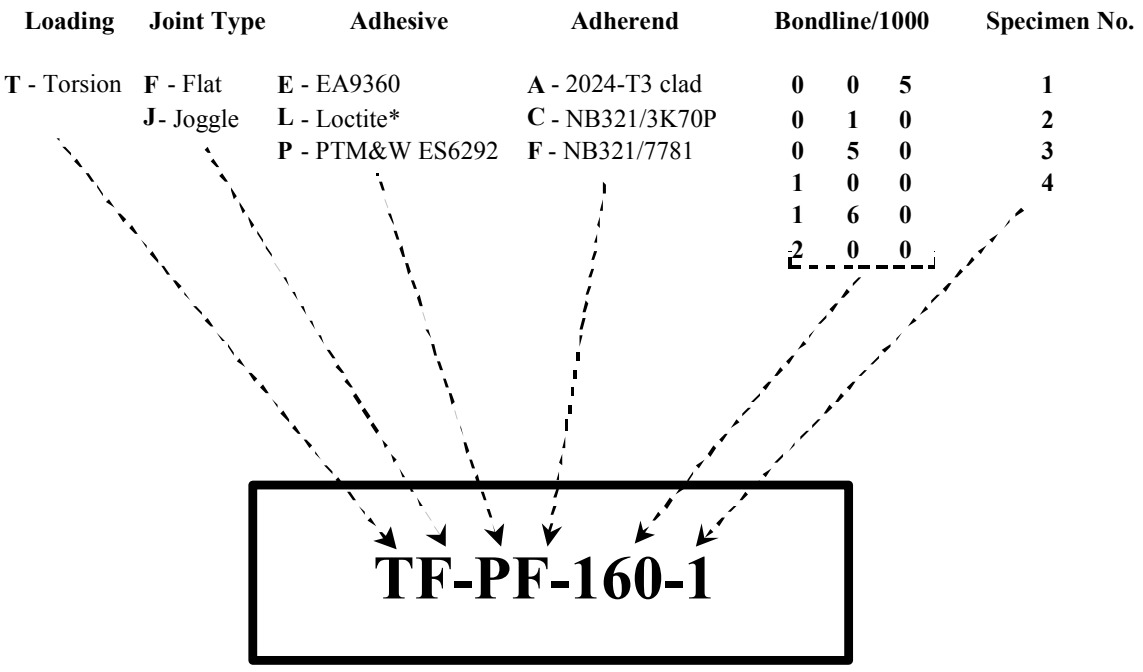

FIGURE 4-4. NOMENCLATURE FOR ADHESIVE TEST SPECIMENS

5. EXPERIMENTAL PROCEDURE.

5.1 DIMENSIONING.

Specimens were dimensioned using digital calipers that automatically recorded the dimensions in a data file. Eight gage thickness readings were recorded along the length of the specimen. In addition, the adhesive thickness was calculated by subtracting two subpanel thicknesses (obtained before specimen fabrication) from the panel thickness after final fabrication. The average of these eight thickness readings was calculated, along with the coefficient of variation, to monitor satisfactory bondline thickness distribution.

5.2 TORSION TEST FIXTURE.

A torsion test fixture was designed to have a maximum capacity of 60,000 in-lbf. It consists of two major sections: fixed- and pivot-end or loading-end. This unique design facilitates torsion-only loading by allowing axial float of the loading-end. A 2.5-inch needle bearing mounted in the loading-end post only allows rotation and translation in the axial direction. A twin-plate moment arm connected by a 2.5-inch shaft through the needle bearing assures that the loading plate does not swivel during the load application. The moment arm has flexibility to change to 6, 9, or 12 inches. All testing in this investigation was conducted with a fixed moment arm of 12 inches. In addition, the swivel end of the actuator has complete rotational degrees of freedom, which prevents any side loads. To ensure that the measured load was orthogonal to the loading plate, the load cell was mounted between the loading plate and the swivel joint of the actuator.

The distance between the loading-end side plate (inboard) and the fixed-end block was approximately 29 inches for this particular test setup. However, this distance can be increased in 24-inch increments without additional fixturing. Slack in the boltholes allows the parts to move in a horizontal direction. Since loading-end and fixed-end bases were separate units, aligning the fixture was a crucial part of testing. A 1-inch hole was drilled through each end-plug assembly and through the fixed-end block so that a 1-inch steel rod could be inserted through these holes to align the fixture. Vertical alignment was achieved using brass shims.

The top half of figure 5-1 shows the test setup for box beam torsion lap shear testing. Both fixed- and loading-end bases were part of the existing edgewise compression and large-scale four-point bend fixtures, respectively. Except the two end plugs and steel channels of the box beam, the parts shown in the bottom half of figure 5-1 were machined using aluminum. Steel channels were machined to have a wall thickness of 0.25 inch. In addition, 0.25-inch doublers at 0.375-inch bolthole locations were added to prevent yielding.

In addition to the specimen modifications (see section 3.3), the 20-ply laminate side plate (Drawing UCSB-BB-060 in appendix A) was replaced by an aluminum side plate with a thickness of 0.125 inch that has similar hole pattern shown in Drawing UCSB-BB-060. A torque wrench was used to bolt specimens to the test fixture to minimize stress concentrations around boltholes and to apply even pressure.

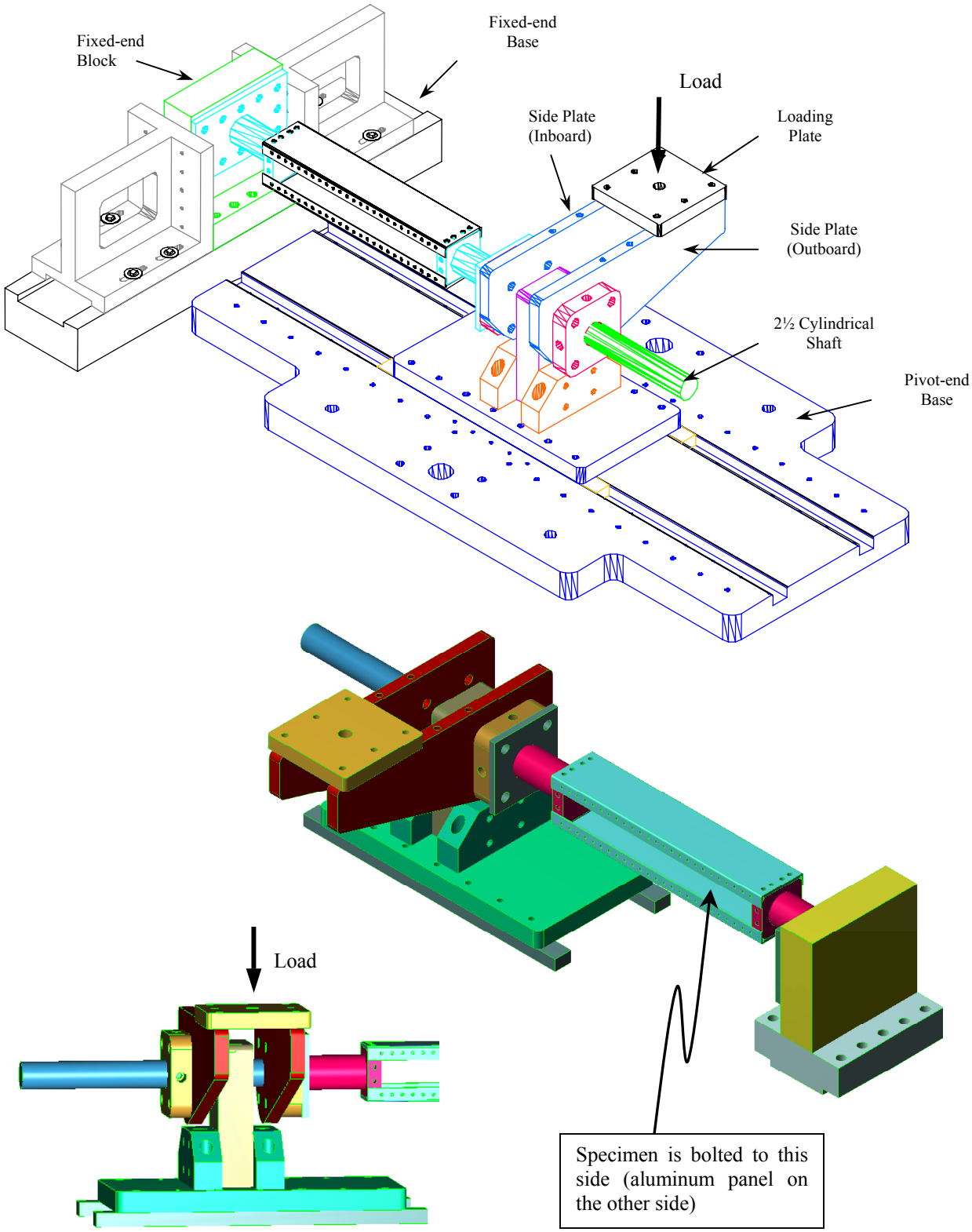

FIGURE 5-1. TEST SETUP FOR ADHESIVE BOX BEAM LAP SHEAR TORSION TEST

5.3 INSTRUMENTATION.

Load and displacement of the actuator were directly recorded onto data files. Load was measured using MTS-calibrated 22-kip load cell. The actuator was controlled by a separate servo-hydraulic test console. Torsion testing was conducted in stroke-control mode with a rate of either 0.075 or 0.10 in/min. FlexTest II™ software was used to control the actuator, while data was acquired using Basic Testware™.

Strain gages manufactured by Measurements Group Inc. were bonded to box beam walls using M-Bond 200 adhesive. In-plane shear strain of the box beam walls and axial strain were obtained from these gages. Since the gage width of the specimen was 0.5 inch, EA-00-125TH-120 rosettes with +45° and -45° gages were used. The steel channels and aluminium side plate used CEA-00-250UR-120 triaxial rosettes. All strain gages were connected to the data acquisition system in MTS-FlexTest command module.

Maximum rotation angle (at the twisting end) of the box beam was measured using a digital level at every 100 lbs. Initial testing indicated highly nonlinear rotation of the box beam. Therefore, a Rotation Variable Differential Transducer manufactured by SENTECH Inc. (Model RVDC15-10N) was mounted to the inner wall of the fixed-end end-cap so that it measured only the maximum rotation of the box beam by isolating any deformation of the test fixture (figure 5-2). In addition, two displacement gages were mounted to the edge of the specimen to measure rotation of the box beam at different locations, as shown in figure 5-2. These were compared with angle calculations using the actuator displacement measured with a linear variable differential transformer and the Principle of Minimum Complimentary Energy (PMCE) predictions.

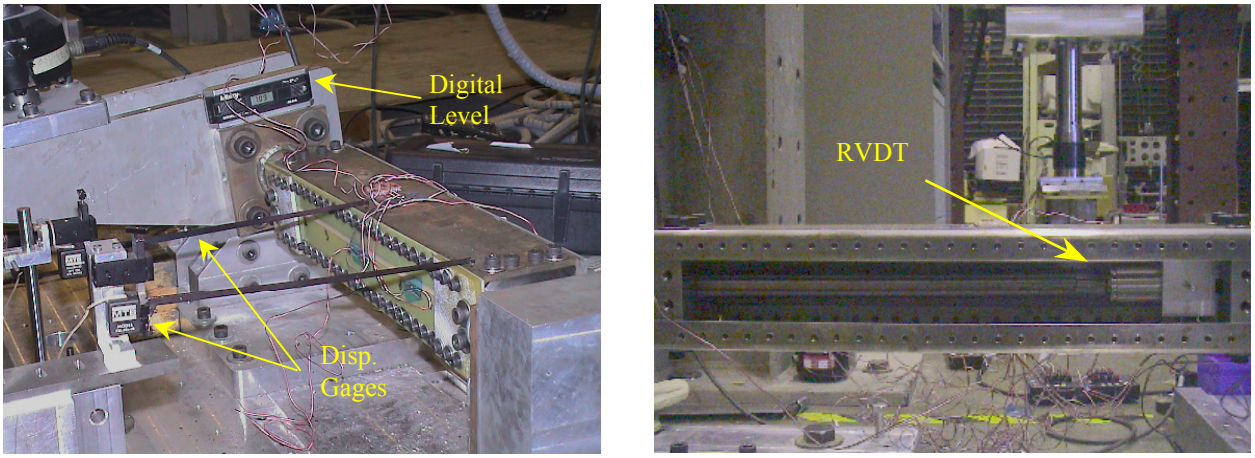

FIGURE 5-2. MEASURING THE MAXIMUM ROTATION OF THE BOX BEAM

5.4 CALIBRATION OF THE TORSION TEST FIXTURE.

The primary goal in this subtask was to validate consistency of the shear flow through each wall of the box beam and then compare the experimental shear flow with theoretical predictions. To calibrate the box beam torsion fixture, two aluminum side panels were mounted to each side

(figure 5-3). These panels were 0.125 inch thick and extended to the full length of the fixture with a hole pattern identical to the 20-ply side panel shown in Drawing UCSB-BB-060 in appendix A. This resulted in a steel-aluminum box beam that has no lap joints. Due to the complexity of the strain field around the lap joint (gage section), it was necessary to replace the joint with an isotropic material so that strain data can be converted into shear flow, as described in section 5.5, to compare with data obtained from steel channels and the other aluminum side plate. An aluminum side plate was chosen so that box beam has similar material on both sides. To test adhesive lap joints, one of these aluminum sides plates was removed and replaced with the joint, as described in section 3.3.

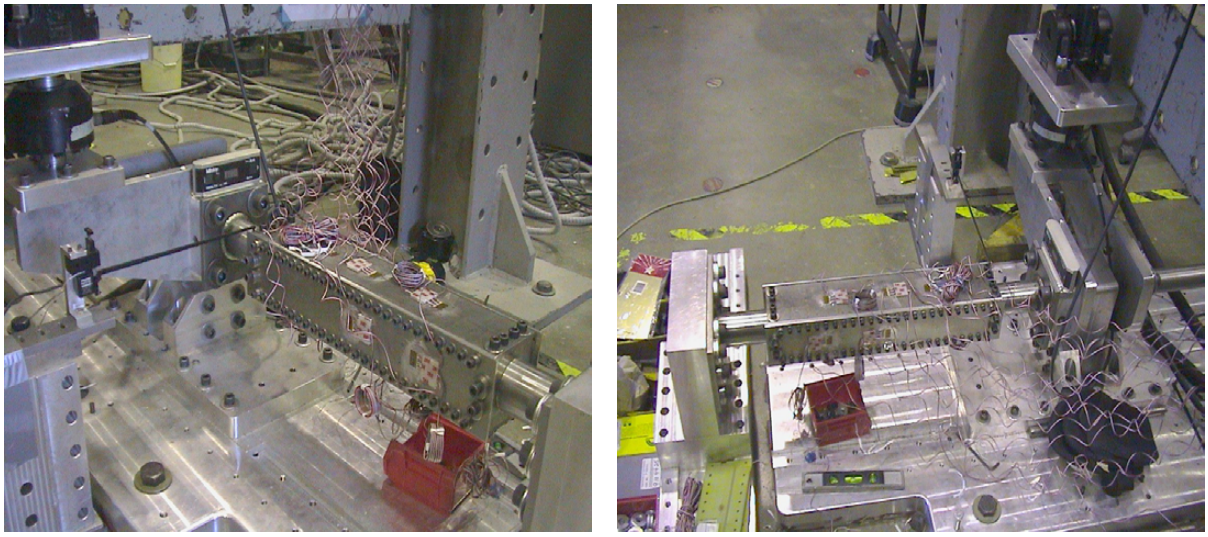

FIGURE 5-3. TEST SETUP FOR CALIBRATION OF THE TORSION FIXTURE

The CEA-06-250UR-120 strain gage rosettes were used to evaluate shear strain. Gages were mounted in such a way to measure the ±45° direction strain with respect to axial direction of the box beam so that the measurements could be converted into shear strain and then to shear flow using the procedure illustrated in section 5.5. The first set of strain gages was mounted at the midpoint (with respect to axial direction) of each side, and the second set was mounted 5 inches away from the center and towards the fixed end. The first letter of each strain gage corresponds to the wall on which it was bonded: Top –T, Bottom –B, Right –R and Left –L (figure 5-4). The second letter indicates location of the gage on each wall: Midpoint–M, Torque end–T and Fixed end–F. Two axial gages were mounted on the top and bottom steel channels towards the fixed end to study effectiveness of the axial float mechanism of the fixture.

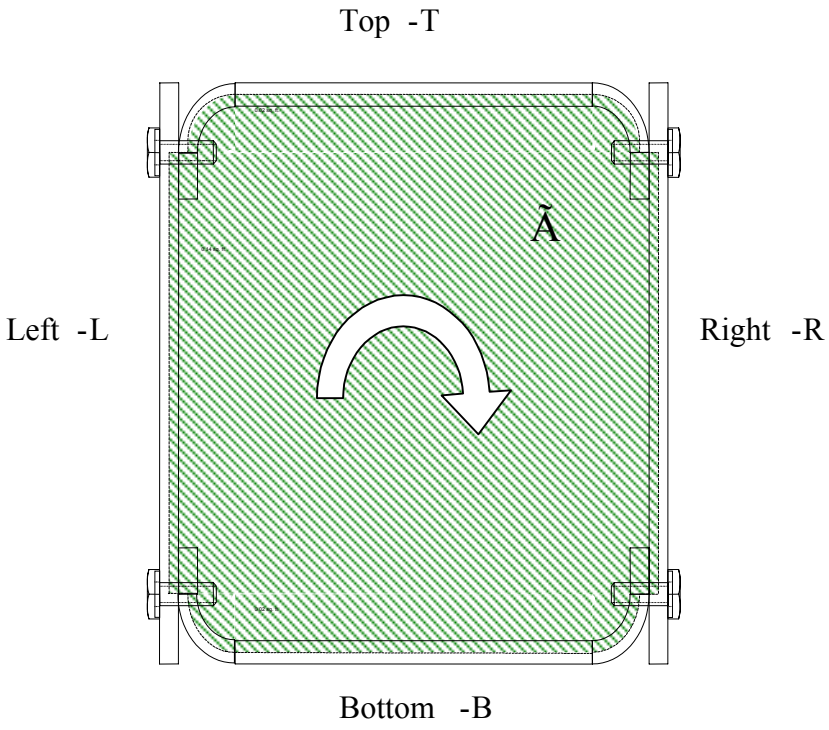

FIGURE 5-4. AREA ENCLOSED BY THE CENTERLINE OF THE CLOSED WALL BOX BEAM CROSS SECTION

5.5 DATA REDUCTION.

Equations 5-1 and 5-2 represent strain data obtained from +45° and -45° strain gages, respectively.

$$\varepsilon_{+45^\circ} = \frac{\varepsilon_x + \varepsilon_y}{2} + \frac{\varepsilon_x - \varepsilon_y}{2} \cdot \cos[2 \cdot (45^\circ)] + \frac{\gamma_{xy}}{2} \cdot \sin[2 \cdot (45^\circ)] \quad (5\text{-}1)$$

$$\varepsilon_{+45^\circ} = \frac{\varepsilon_x + \varepsilon_y}{2} + \frac{\varepsilon_x - \varepsilon_y}{2} \cdot \cos[2 \cdot (-45^\circ)] + \frac{\gamma_{xy}}{2} \cdot \sin[2 \cdot (-45^\circ)] \quad (5\text{-}2)$$

Subtracting equations 5-1 and 5-2 and rearranging terms yields to the following:

$$\gamma_{xy} = \varepsilon_{45^\circ} - \varepsilon_{-45^\circ} \quad (5\text{-}3)$$

Using equation 5-3, strain data obtained from ±45° strain gage rosettes were converted into corresponding shear strain.

The Bredt-Batho theory [9], a theory of torsion of closed thin-walled beams, was used to calculate shear flow through box beam walls assuming that (a) stresses do not vary through the thickness and (b) direction in which the stress acts is tangent to the median line drawn through the wall thickness.

It is imperative that the load case is pure torsion for application of these formulas. Shear flow throughout the cross section of the box beam, q, and the average shear stress acting over the thickness of each wall, σ_{xs}, are given in equations 5-4 (Bredt-Batho Formula) and 5-5 (for thin-walled beams). The mean area enclosed within the boundary of the centerline of box beam wall thickness, $\tilde{A}$, was calculated, as shown in figure 5-4.

$$q = \frac{T}{2.\tilde{A}} \tag{5-4}$$

$$\sigma_{xs} = \frac{q}{t} \tag{5-5}$$

Using Hooke's Law, shear stress, σ_{xs}, in the linear elastic range is expressed in equation 5-6.

$$\sigma_{xs} = G_{xs}\,\gamma_{xs} \tag{5-6}$$

Note that the y subscript in equation 5-3 was replaced by s to denote (in-plane) transverse direction of each wall. Substituting equations 5-3 and 5-6 into equation 5-5 yields to equation 5-7, which is valid only in the linear elastic range.

$$q = G_{xs}\,\gamma_{xs} t \tag{5-7}$$

The measured data were compared with the maximum rotation estimated by the PMCE. The maximum rotation (angle of twist) in radian derived from PMCE is given in equation 5-8 for box beam.

$$\phi = \frac{T \cdot L}{4 \cdot \tilde{A}^2} \cdot \left(2 \cdot \frac{s_{steel}}{G_{steel} \cdot t_{steel}} + \frac{s_{right}}{G_{right} \cdot t_{right}} + \frac{s_{left}}{G_{left} \cdot t_{left}} \right) \tag{5-8}$$

where G and t represent the shear modulus and the thickness of each wall, respectively, and L represents the length of box beam between end-cap bolts. In addition, s represents the length along the centerline of each wall. Please note that equation 5-8 assumes linear elastic behavior of materials.

To compare shear flow calculation given by equation 5-4, strain gage data were converted to shear flow of each wall using equation 5-7. Lap joint was assumed to be a single panel with 20 plies of fiberglass/carbon laminate (or a 0.10-inch-thick solid aluminum panel for Loctite-aluminum specimens).

5.6 FAILURE MODES.

To gain a full understanding of the adhesive and joint characteristics being investigated, the mode of failure must be evaluated. In adhesive technology, there are three primary characterizations for failure of an adhesive joint (figure 5-5):

- Cohesive Failure is characterized by failure of the adhesive itself.

- Adhesive Failure is characterized by a failure of the joint at the adhesive and adherend interface and is typically caused by inadequate surface preparation, chemically or mechanically. Specimens that fail adhesively tend to have excessive peel stresses that lead to failure and often do not yield a strength value for the adhesive joint but rather indicate unsuitable surface qualities of the adherend.

- Substrate Failure is characterized by failure of the adherend instead of the adhesive. In metals, this occurs when the adherend yields. In composites, the laminate typically fails by way of interlaminar failure, i.e., when the matrix between plies fails. In substrates, failure occurs when the adhesive is stronger than the adherend in the joint being tested. Therefore, this failure mode is characterized as a joint failure, rather than an adhesive failure.

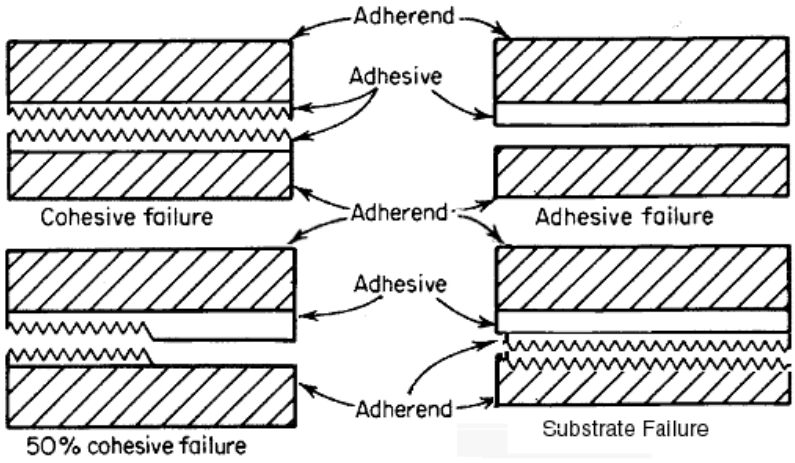

FIGURE 5-5. FAILURE MODES OF ADHESIVE TEST SPECIMENS

In coupon level testing that have small gage sections such as for ASTM D 5656 specimens, these failure modes can easily be identified and categorized. However, the specimen geometry under investigation has a gage length of 17.25 inches. Therefore, a combination of several failure modes can be observed in different locations of the gage section. In addition, bearing and shear-buckling failures are possible for the test setup used in this investigation. However, those two failure modes are not part of this study.

6. RESULTS AND DISCUSSION.

6.1 CALIBRATION TEST RESULTS.

Calibration of the test fixture with aluminum plates on both sides indicated constant shear flow through all four box beam walls, i.e., shear flow calculated using equation 5-7 for each wall was equal (figure 6-1). In addition, these values were comparable with the experimental shear flow obtained using equation 5-4. Axial strain data indicated insignificant values, confirming negligible axial forces. A displacement gage placed at the fixed end of the test fixture indicated insignificant rotations as expected. Further, shear strain data indicated linear elastic behavior up to a torque of 25,000 in-lbf, which was comparable to a shear flow of approximately 800 lbf/in. However, the maximum rotation data at torque end indicated highly nonlinear and significantly higher magnitudes than the values predicted by the PMCE (figure 6-2). Nevertheless, strain data recorded on steel and aluminum walls indicated close to linear elastic behavior (figure 6-3), indicating that the nonlinear rotation could have been caused by the nonlinear deformation of the fixture-to-specimen bolted joints.

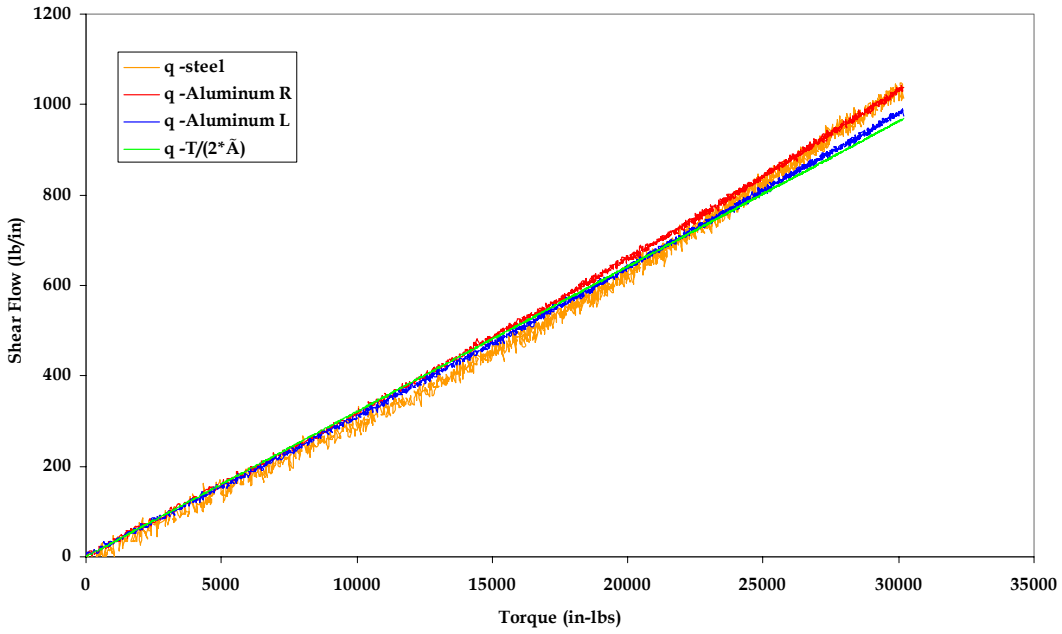

FIGURE 6-1. SHEAR FLOW DATA FOR TEST FIXTURE CALIBRATION

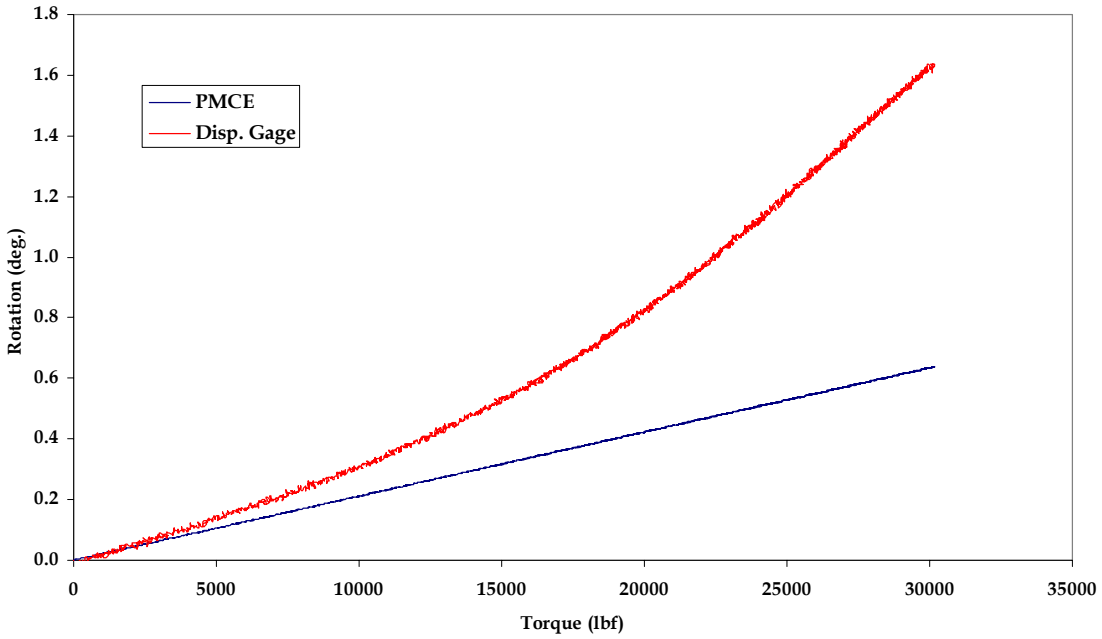

FIGURE 6-2. MAXIMUM ROTATION OF CALIBRATION TEST

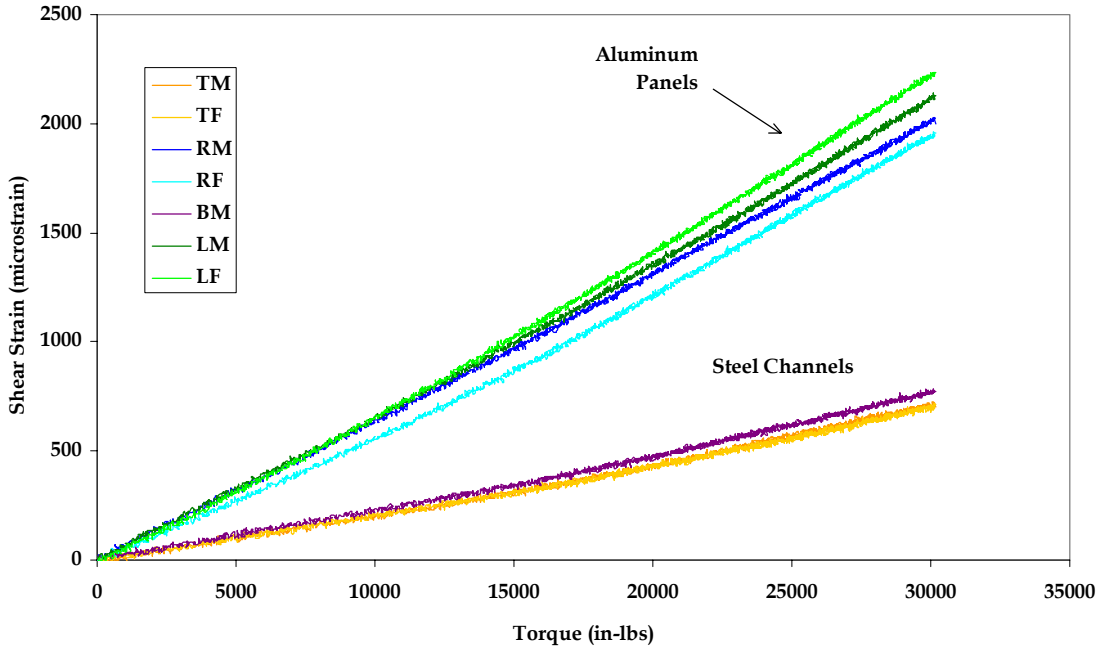

FIGURE 6-3. SHEAR STRAIN DATA FOR CALIBRATION TEST

6.2 TEST RESULTS FOR FLAT JOINTS.

Table 6-1 summarizes test results obtained for flat-joint specimens in Phase I. Specimens that had bondline thicknesses of 0.01 inch were aborted after the test reached the maximum load capacity of the fixture. Thus, test results for specimens with bondline thickness of 0.01 inch were excluded in this report. Figure 6-4 shows a comparison of average maximum applied torque for each bondline thickness based on test results shown in table 6-1. Load-carrying capability of lap joints decreased for thicker bondlines. This observation was noted in coupon level testing as well as references 10 and 11. In addition, maximum rotation before failure was dropped significantly for thicker bondlines (figure 6-5). This was explained by the significantly short plastic strain development range and the low yield stress of thick bondlines compared to thin bondlines (figure 2-1).

Table 6-2 compares maximum shear flow obtained for specimens in Phase I from the Bredt-Batho Formula (Experimental) and SLBJ theory (Purdue Analysis). SLBJ shear flow data were predicted based on the thicknesses available from ASTM D 5656 characteristic shear responses (section 2.5). Therefore, SLBJ predictions were linearly curve fitted (figure 6-6), and a representative equation was derived to obtain analytical approximations for corresponding bondline thicknesses presented in table 6-2. ASTM D 5656 data were not available for bondline thicknesses beyond 0.168 inch. Therefore, no comparisons were performed for 0.20-inch specimens. Figure 6-6 graphically compares the experimental maximum shear flow and SLBJ predictions with respect to bondline thickness. The load-carrying capability of lap joints decreased for thicker bondlines as predicted by SLBJ theory. This observation was noted in coupon level testing as observed in references 5 and 10. Figure 6-6 graphically compares maximum shear flow data obtained from analysis and experiment with respect to bondline thickness. The rate of joint strength drop for increasing bondline thickness for SLBJ predictions was higher than that of experimental data. This resulted in higher experimental failure strengths than SLBJ predictions for thick bondlines. Linear regression presented in figure 6-6 for experimental data and SLBJ predictions indicates that the SLBJ predictions were 4.2%, 9.1%, 15.1%, and 22.4% lower than the average experimental data for bondline thickness of 0.05, 0.10, 0.16, and 0.20 inches, respectively.

Unlike both steel and aluminum side plate, the in-plane shear strains recorded on the overlap region, especially for thin bondlines, indicated a significant nonlinearity. Average failure strains of outer adherend calculated using equation 5-6 for each bondline thickness are superimposed on a in-plane shear stress-strain curve obtained from a test conducted, according to ASTM D 5379, for a 20-ply ($[0_4/45/-45/0_4]_s$) laminate in figure 6-7. Failure strains indicated that the adherend had exceeded the linear elastic limit of FG7781 fiber glass. The SLBJ predictions assumed linear elastic behavior of the adherend. However, failure strains indicated that the adherend had exceeded the linear elastic limit of the laminate, which may have caused the nonlinearity in the lap joint strain data. For a 0.05-inch bondline, the failure strains were substantial and the specimens resulted in adherend failure. Therefore, the comparison of the SLBJ predictions with experimental data for these specimens might be misleading.

TABLE 6-1. TEST RESULTS FOR ES6292-FG7781 FLAT-JOINT SPECIMENS (PHASE I)

Specimen Name	Bondline Thickness (in.)	Test Speed (in/min)	Bolt Torque (in-lbf)	Failure Load (lbf)	Maximum Torque (in-lbf)	Maximum Rotation (deg.)	Statistical Data	Torque (in-kip)	Rotation (deg.)
TF-PF-050-1	0.0505	0.100	100	5270.55	63246.56	8.21	Average	57.30	7.01
TF-PF-050-2	0.0493	0.100	100	5006.18	60074.16	6.75	STD	5.38	0.92
TF-PF-050-3	0.0519	0.100	100	4273.05	51276.59	6.00	COV	9.38	13.14
TF-PF-050-4	0.0464	0.100	100	4549.17	54589.99	7.06			
TF-PF-100-1	0.1022	0.075	125	4228.19	50738.24	5.13	Average	53.10	5.69
TF-PF-100-2	0.0926	0.075	125	4516.89	54202.71	6.13	STD	2.68	0.42
TF-PF-100-3	0.1057	0.075	125	4696.49	56357.92	5.76	COV	5.04	7.31
TF-PF-100-4	0.1055	0.075	125	4256.72	51080.66	5.73			
TF-PF-160-1	0.1606	0.075	125	3216.88	38602.56	4.30	Average	39.49	4.00
TF-PF-160-2	0.1557	0.075	125	3404.03	40848.42	3.98	STD	1.05	0.22
TF-PF-160-3	0.1587	0.075	125	3314.23	39770.81	3.92	COV	2.65	5.45
TF-PF-160-4	0.1554	0.075	125	3227.79	38733.48	3.79			
TF-PF-200-1	0.2024	0.075	125	3055.74	36668.91	3.22	Average	38.66	3.80
TF-PF-200-2	0.2011	0.075	125	3699.45	44393.44	4.67	STD	3.83	0.63
TF-PF-200-3	0.2001	0.075	125	3049.03	36588.34	3.51	COV	9.90	16.47
TF-PF-200-4	0.1993	0.075	125	3082.60	36991.18	3.78			

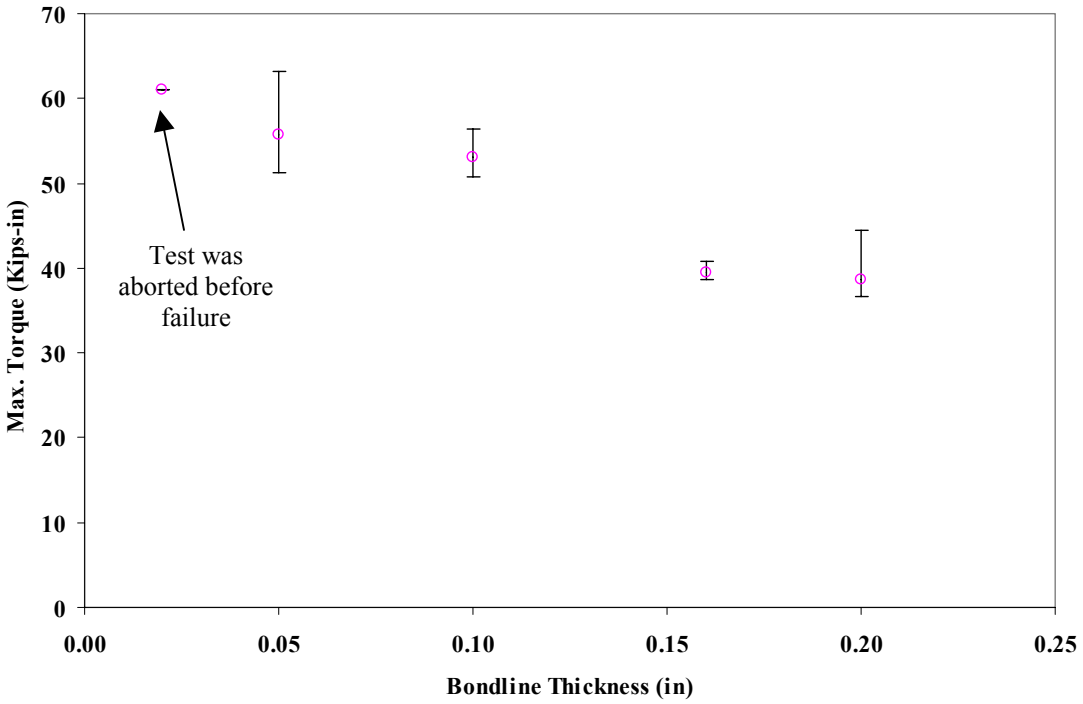

FIGURE 6-4. COMPARISON OF AVERAGE MAXIMUM TORQUE APPLIED (PHASE I)

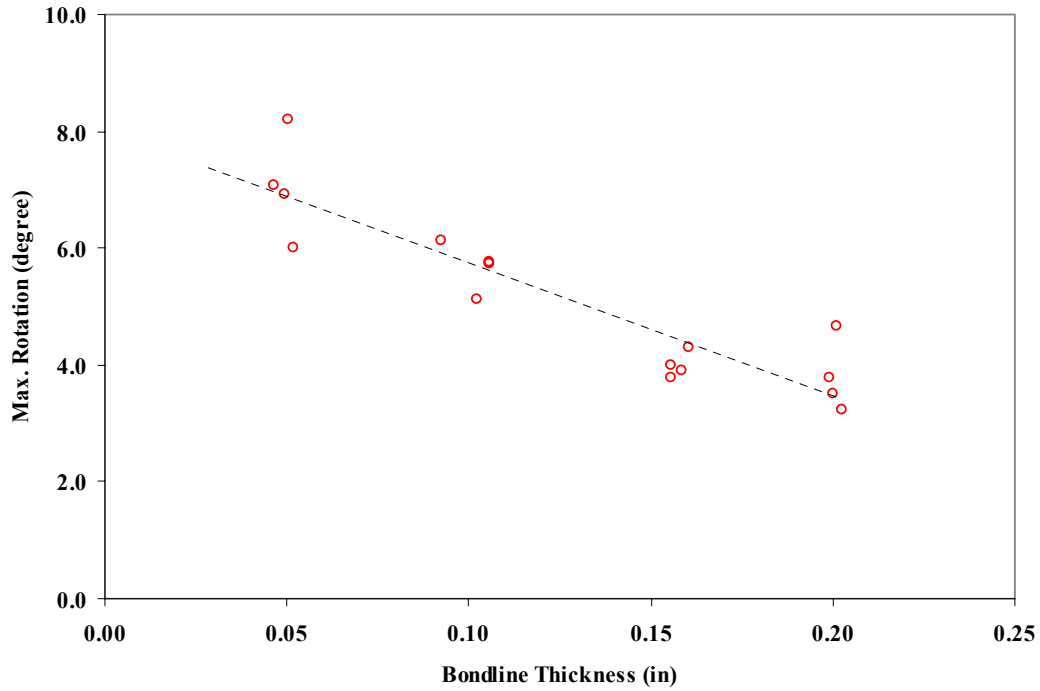

FIGURE 6-5. MAXIMUM ROTATION RECORDED AT THE LOADING END OF THE TEST FIXTURE FOR ES6292-FG7781

TABLE 6-2. COMPARISON OF SHEAR FLOW FOR ES6292-FG7781 FLAT-JOINT SPECIMENS (PHASE I)

Specimen Name	Bondline Thickness (in.)	Maximum Shear Flow (lbf/in)		Statistical Data	Maximum Shear Flow (lbf/in)	
		Experimental	SLBJ		Experimental	SLBJ
TF-PF-050-1	0.0505	2019.29	1707.92	Average	1779.20	1713.70
TF-PF-050-2	0.0493	1717.50	1714.91	STD	166.29	14.03
TF-PF-050-3	0.0519	1637.12	1699.47	COV	9.35	0.82
TF-PF-050-4	0.0464	1742.91	1732.50			
TF-PF-100-1	0.1022	1619.93	1395.78	Average	1695.17	1399.82
TF-PF-100-2	0.0926	1730.54	1453.63	STD	85.44	37.20
TF-PF-100-3	0.1057	1799.35	1374.33	COV	5.04	2.66
TF-PF-100-4	0.1055	1630.86	1375.54			
TF-PF-160-1	0.1606	1232.47	1042.74	Average	1260.77	1060.829
TF-PF-160-2	0.1557	1304.18	1072.35	STD	33.40	14.990
TF-PF-160-3	0.1587	1269.77	1054.30	COV	2.65	1.413
TF-PF-160-4	0.1554	1236.65	1073.93			
TF-PF-200-1	0.2024	1170.74	N/A	Average	1234.32	ASTM D 5656 data were not available
TF-PF-200-2	0.2011	1417.36	N/A	STD	122.15	
TF-PF-200-3	0.2001	1168.16	N/A	COV	9.90	
TF-PF-200-4	0.1993	1181.03	N/A			

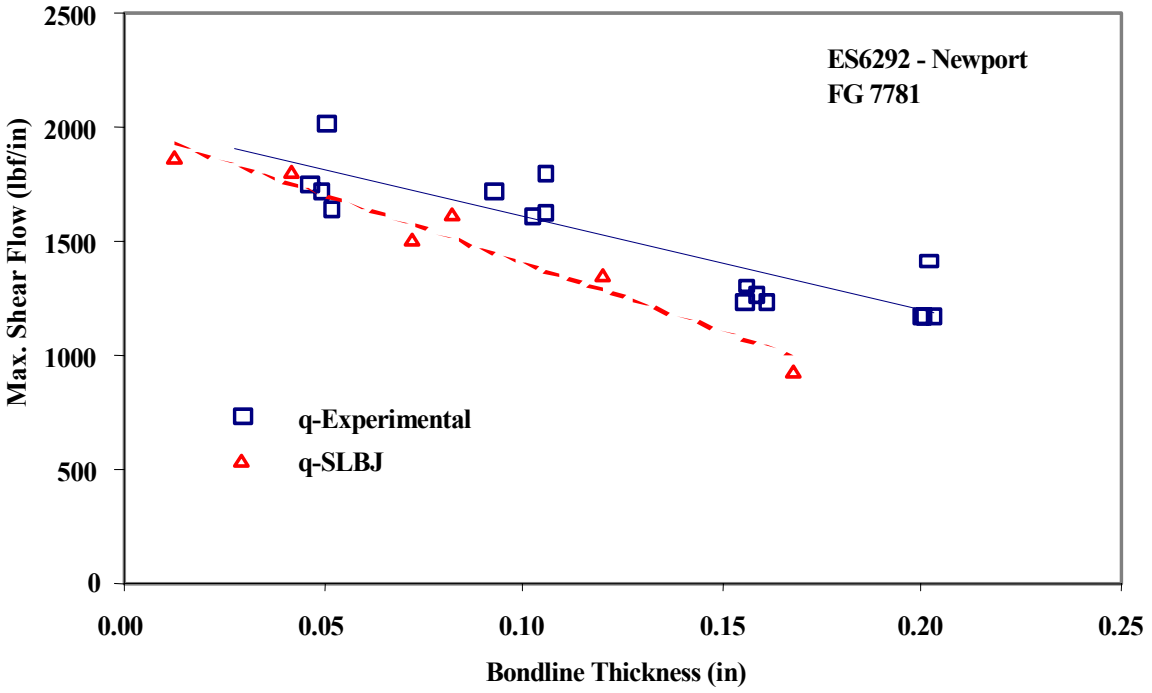

FIGURE 6-6. MAXIMUM SHEAR FLOW OF ES6292-FG7781 FLAT-JOINT SPECIMENS

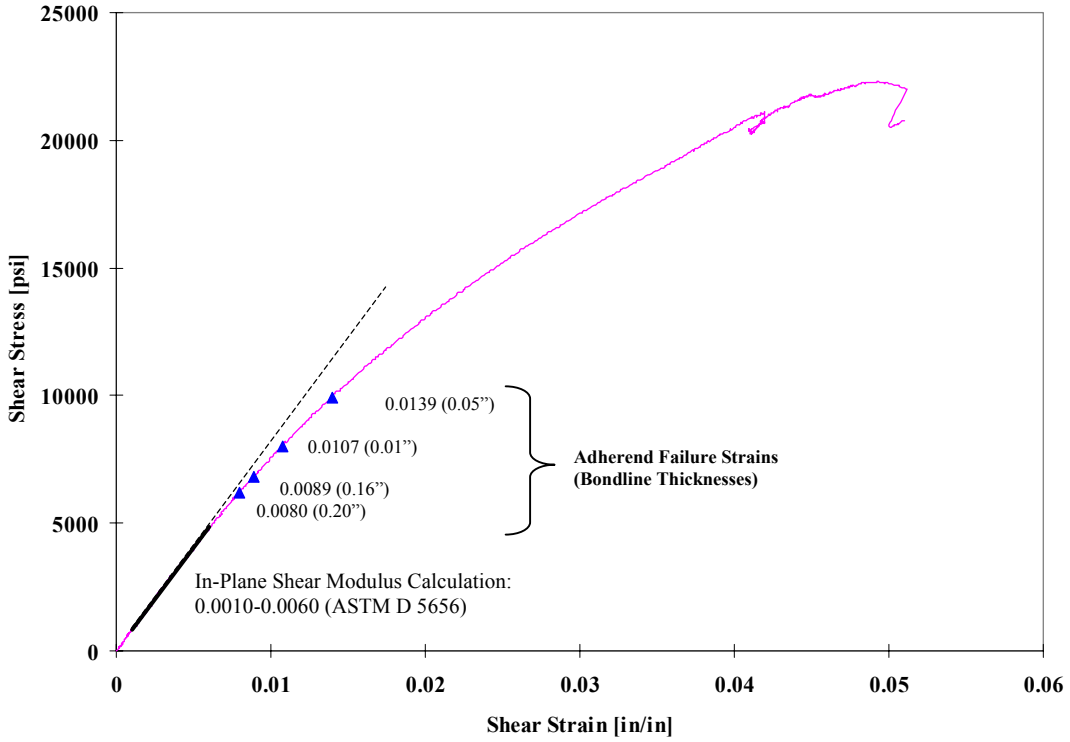

FIGURE 6-7. AVERAGE FAILURE STRAINS OF OUTER ADHEREND SUPERIMPOSED ON AN IN-PLANE SHEAR STRESS-STRAIN CURVE OF A 20-PLY LAMINATE

Test results for Phase II are depicted in table 6-3, and shear flow results for both flat and joggle joints are compared in table 6-4. Test results of specimen TF-EC-100-4 were excluded in the statistics due its premature failure, which was identified as inadequate clamp force during panel fabrication, resulting in a deficient bonding between adhesive-adherend interface. The experimental shear flow was significantly lower than SLBJ predictions. Failure mode analysis (section 6.4) of these joints revealed a possible cause for this observation. Failure modes for EA9360 specimens, except for specimen TF-EC-100-4, were adherend failures, in which at least one ply was attached to the adhesive layer and there was no indication of fracture. Therefore, failure load indicated for these joints may not reflect actual adhesive failure, but failure of the adherend, which was below the failure of the adhesive. In standard joint design practices, whenever possible, the joint is designed to ensure that the adherends fails before adhesive [12]. This is because failure in the adherends is fiber controlled (the failure starts with fabric failure that allows the crack to propagate to the interlaminar plane), while failure in the adhesive is resin dominated and, thus, subject to effects of voids and other defects, thickness variations, environmental effects, processing variations, deficiencies in surface preparation, and other factors that are not always adequately controlled.

Loctite joint results indicate that the SLBJ predictions were within 8% of the experimental shear flow. However, shear flow obtained from strain gage data was significantly higher than SLBJ predictions. Shear buckling of the adherend caused strain gage data to increase significantly, in turn causing q-strain (equation 5-7) to be higher than SLBJ predictions. These joints failed by adherend shear buckling and adhesive peel. Therefore, the failure strength comparison can be misleading, because the SLBJ theory predicted the failure of the adhesive by assuming linear elastic behavior of the adherend. Aluminum adherends used in these specimens were relatively thin, and analyses show that for such cases, stresses in the adhesive will be small enough to guarantee that the adherends will reach their load capacity before failure can occur in the adhesive [12].

Shear flow along gage length based on strain gage data of 0.16-inch specimens indicates a somewhat constant distribution along the gage length (figure 6-8). In addition, average shear flow obtained from both SLBJ and experimental data for all flat and joggle joints are compared in figure 6-9.

6.3 TEST RESULTS FOR JOGGLE JOINTS.

Joggle joints tested in Phase I failed in bearing at opposite-side corner boltholes. Those results were excluded in comparison. The results for EA9360-carbon joggle joints indicated no significant changes compared to flat joints (figure 6-10). Failure modes indicate adherend failure, as observed on flat joints. Joggle joints indicated somewhat higher strength compared to flat joints. This observation can be explained by extra adhesive left between joggle and flat adherend, as shown in figure 3-5, which increased the bonded surface area. As observed for flat EA9360 specimens, SLBJ predictions for EA9360 joggle joints were substantially higher than the experimental data (figure 6-9). Adherend failure in joggle specimens may have caused premature failure of these joints.

TABLE 6-3. TEST RESULTS FOR SPECIMENS IN PHASE II

Specimen Name	Bondline Thickness (in)	Failure Load (lbf)	Maximum Torque (in-lbf)	Maximum Rotation (deg.)	Statistical Data	Torque (in-kip)	Rotation (deg.)
TF-LA-050-01	0.0658	3923.92	47087.01	5.61	Average	46.03	5.34
TF-LA-050-02	0.0662	3747.67	44972.08	5.08	STD	1.50	0.38
					COV	3.25	7.10
TF-EC-100-01	0.1005	3648.64	43783.68	6.86	Average	44.13	4.59
TF-EC-100-02	0.1012	3928.11	47137.36	4.95	STD	2.85	0.51
TF-EC-100-03	0.0999	3455.61	41467.33	4.23	COV	6.46	11.02
TF-EC-100-04	0.1278	Premature Failure					
Joggle Joint Results							
TJ-EC-090-01	0.0930	3876.92	46523.02	4.77	Average	48.81	5.16
TJ-EC-090-02	0.0938	4257.94	51095.31	5.56	STD	3.23	0.56
					COV	6.62	10.78
TJ-EC-130-01	0.1359	3718.30	44619.59	4.71	Average	44.75	4.89
TJ-EC-130-02	0.1326	3739.28	44871.37	5.06	STD	0.18	0.25
					COV	0.40	5.19

NOTE: All specimens failed in adherend failure mode, which is characterized as a joint failure, rather than failure of the adhesive.

TABLE 6-4. COMPARISON OF SHEAR FLOW FOR SPECIMENS IN PHASE II

Specimen Name	Bondline Thickness (in)	Maximum Shear Flow (lbf/in)		Statistical Data	Maximum Shear Flow (lbf/in)	
		Experimental	SLBJ		Experimental	SLBJ
TF-LA-050-01	0.0658	1514.97	1559.14	Average	1480.94	1560.24
TF-LA-050-02	0.0662	1446.92	1561.33	STD	48.12	1.55
				COV	3.25	0.10
TF-EC-100-01(r)	0.1005	1397.89	1994.42	Average	1408.93	1994.16
TF-EC-100-02	0.1012	1504.96	1989.72	STD	91.02	4.32
TF-EC-100-03	0.0999	1323.94	1998.34	COV	6.46	0.22
TF-EC-100-04	0.1278	Premature Failure				
Joggle Joint Results						
TJ-EC-090-01	0.0930	1485.35	2041.22	Average	1558.34	2038.948
TJ-EC-090-02	0.0938	1631.33	2036.68	STD	103.22	3.215
				COV	6.62	0.158
TJ-EC-130-01	0.1359	1424.58	1772.42	Average	1428.60	1782.81
TJ-EC-130-02	0.1326	1432.62	1793.20	STD	5.68	14.69
				COV	0.40	0.82

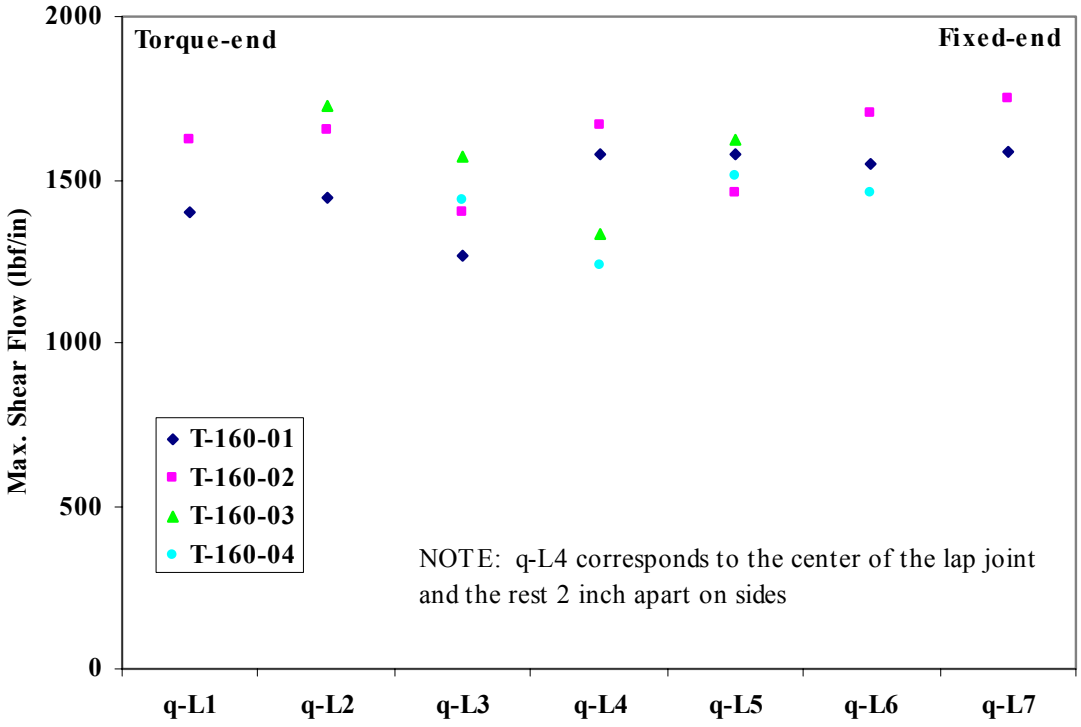

FIGURE 6-8. MAXIMUM SHEAR FLOW ALONG GAGE LENGTH OF 0.16-in.-THICK BONDLINE SPECIMENS

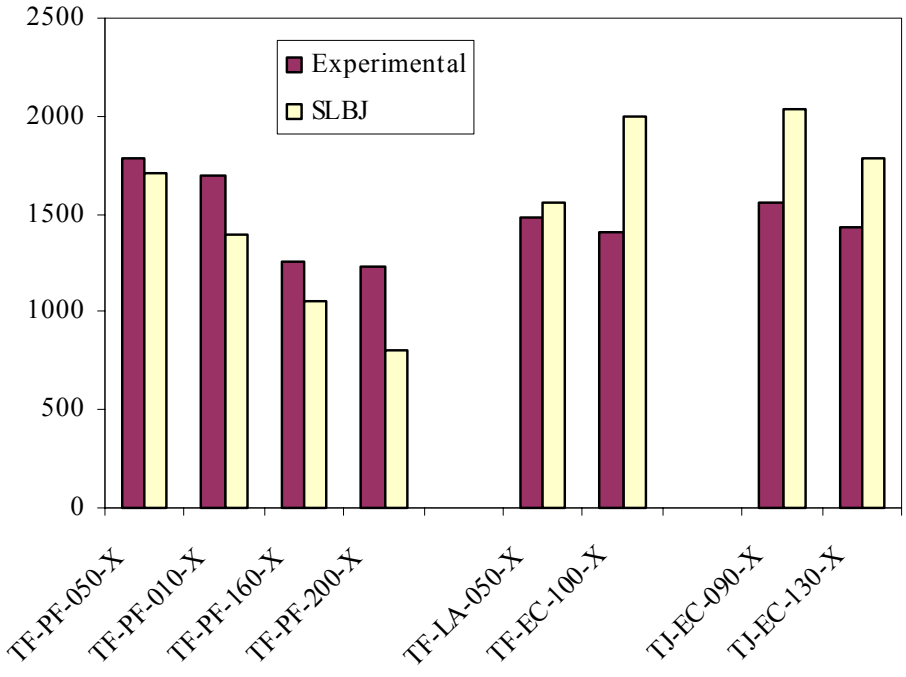

FIGURE 6-9. COMPARISON OF AVERAGE SHEAR FLOW DATA

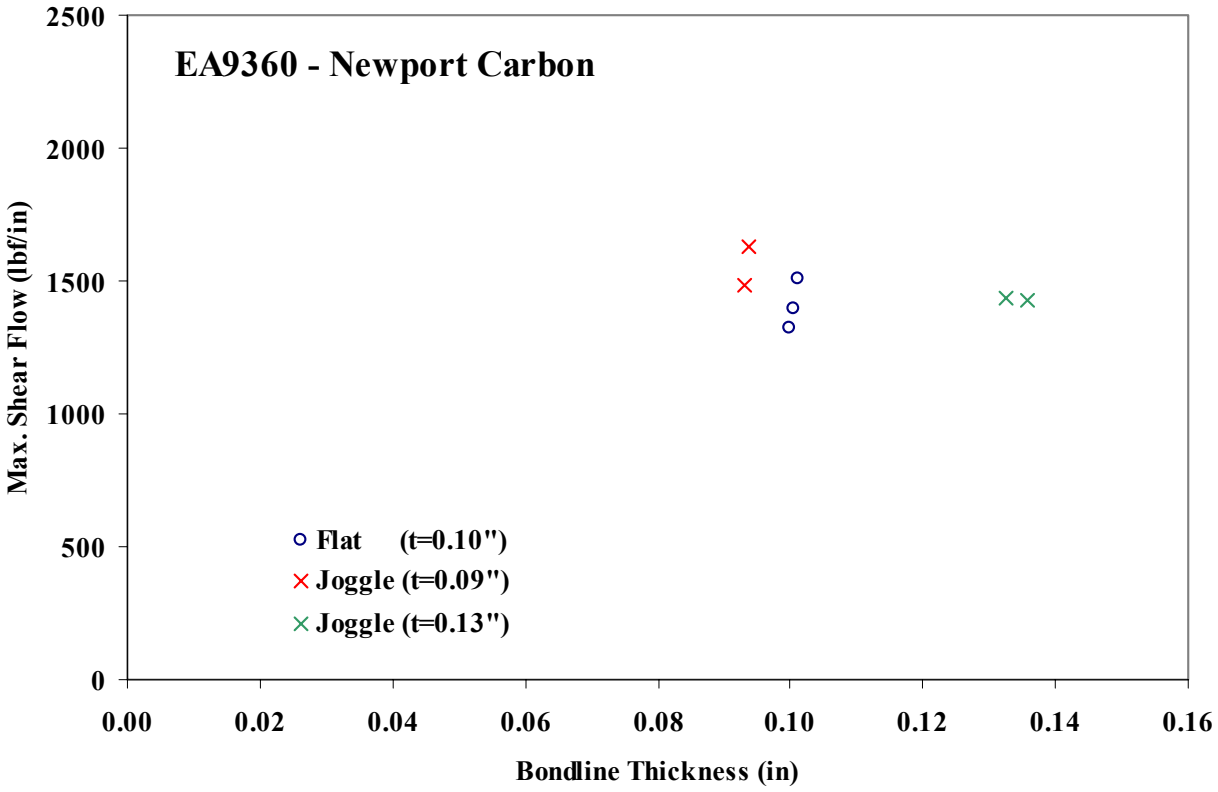

FIGURE 6-10. MAXIMUM SHEAR FLOW COMPARISON OF EA9360-CARBON SPECIMENS

6.4 FAILURE MODES.

Most of the ES6292 specimens indicated combinations of failure modes depicted in figure 6-11. Failure modes indicated significant changes as bondline thickness increased. Photogrammetry and Electronic Speckle Pattern Interferometry (ESPI) were explored to determine the failure initiation. The ESPI technique was found to be excessively sensitive to severe rigid body motion in torsion testing and resulted in confusion in the data. Photogrammetry, using the ARAMIS system, indicated anomalies closer to loading end of the specimen, as shown in figure 6-12(b). However, sensitivity of the ARAMIS system was incapable of capturing these anomalies towards failure, as shown in figure 6-12(c).

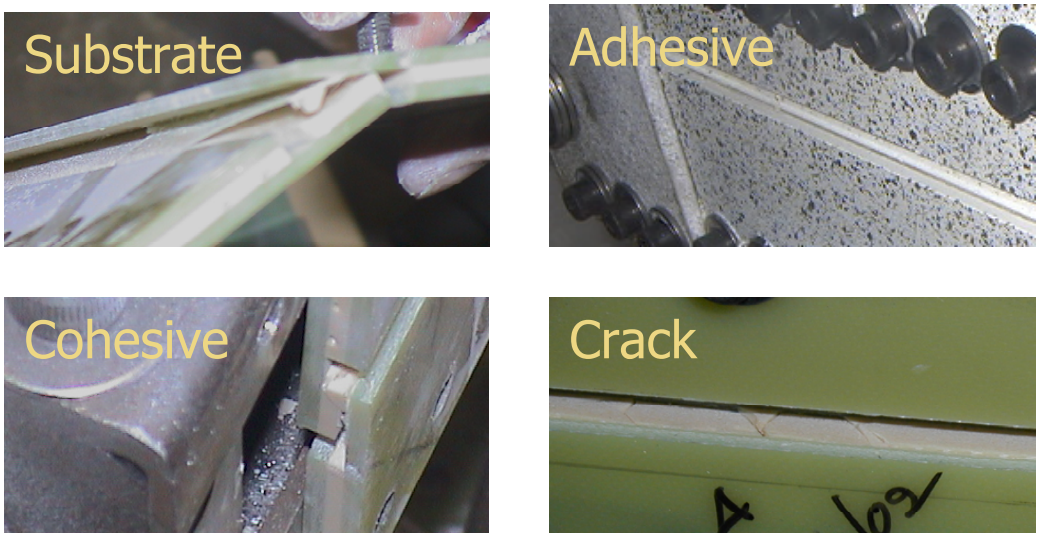

FIGURE 6-11. FAILURE MODES OF ES6292-FG7781 FLAT-JOINT SPECIMENS

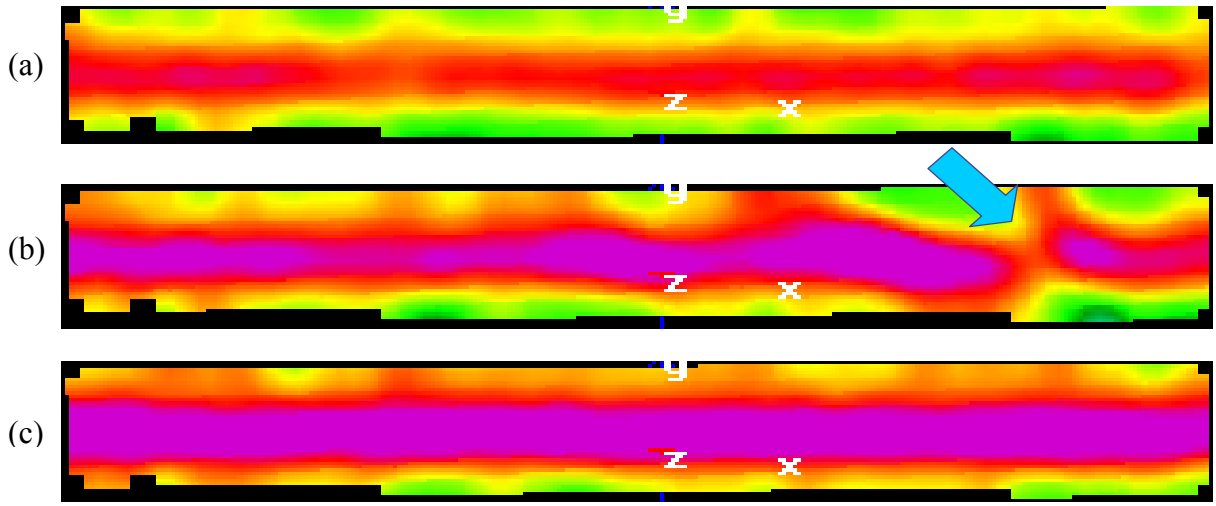

FIGURE 6-12. FAILURE INITIATION INVESTIGATION USING PHOTOGRAMMETRY

Failure analysis of thin joints indicated possible failure initiation at the loading end (substrate failure), while for thick bondlines, it was a combination of cohesive and adhesive failures in the midsection of the joint. Each specimen was carefully examined to determine primary failure modes. From the failure analysis, figure 6-13 shows the primary failure mode of ES6292 specimens. Thin adhesive bondlines indicated higher failure loads that may have been in close proximity to the ultimate loads of the adherend, i.e., interlaminar shear strength. Substrate failure observed at the loading end of each 0.05-inch specimen indicated that this may be the primary mode of failure. Extensive coupon level testing conducted in reference 11 also revealed first-ply failure of the substrate due to interlaminar failure for thin bondlines. The ASTM D 5656 data shows that apparent shear strain at failure is significantly higher for thin bondlines

than that of thick bondlines, indicating an accumulation of substantial plastic strain before failure of thin bondlines [13]. For box beam torsion testing, the high angle of twist data gathered for thin bondlines also concurred with this assessment. As a result, the adherends experienced substantial strains, which consequently resulted in interlaminar failure. As the bondline increased, the adhesive yielding occurred at lower stress levels compared to thin bondlines and there was virtually no plastic strain accumulation before failure, resulting in an unstable damage development process. Therefore, thick bondlines resulted in adhesive cracking in multiple locations with a cohesive-type failure and lower failure strengths than the thin bondlines.

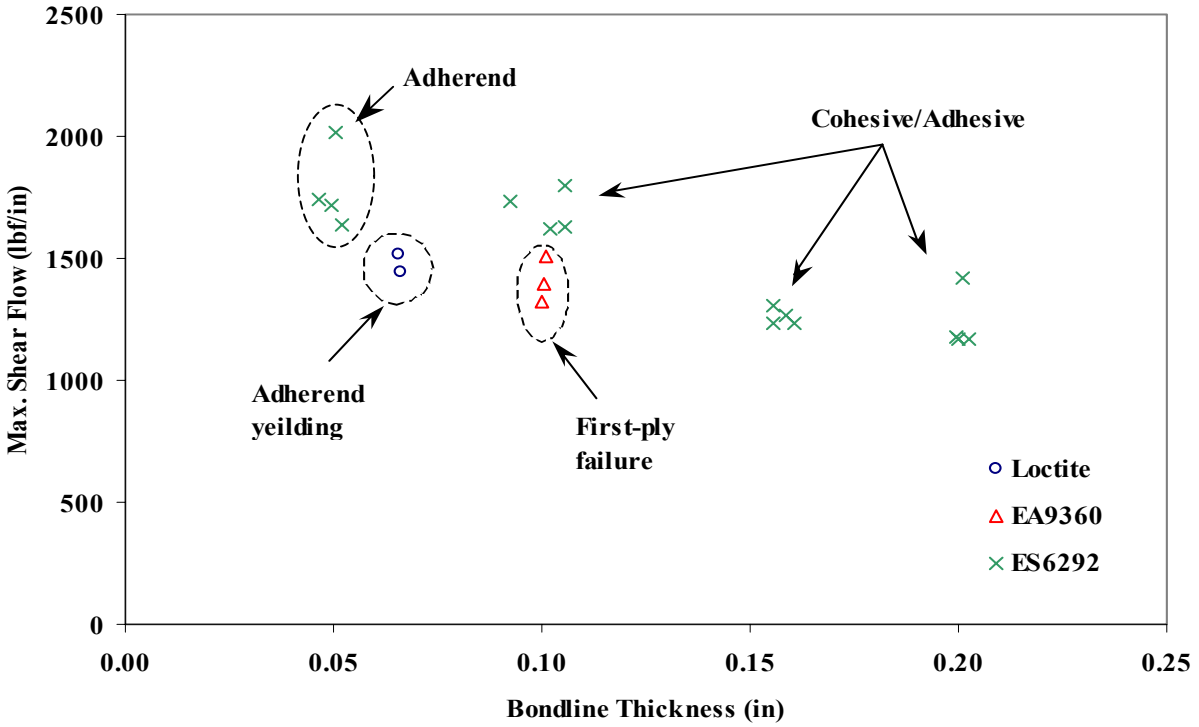

FIGURE 6-13. MAXIMUM SHEAR FLOW AND FAILURE MODE COMPARISON OF ALL ADHESIVES

Both flat and joggle EA9360 joints indicated first-ply failure and no noticeable damage to the adhesive layer. However, these thick bondlines resulted in adherend failure, contradicting the conclusions based on observations in the failure analysis of Phase I results. Though the stiffness of EA9360 is comparable with ES6292, the plastic strain accumulation of EA9360-thick bondlines was more stable than that of ES6292. Thus, the failure strain of EA9360 was higher than that of ES6292. In addition, the interlaminar shear strength of carbon cloth was lower than that of FG7781 E-glass fabric. Combining these adhesive-adherend material properties may be the possible cause of the adherend failure of EA9360 joints. This mode is considered a bonded joint failure rather than an adhesive failure.

Loctite specimens indicated significant shear buckling that resulted in adherend yielding and adhesive peeling at specimen edges (figure 6-14). Typically, this leads to a catastrophic failure of the joint, as seen in both ES6292 and EA9360 adhesives. However, the ductility and large plastic strain accumulations at lower stress levels of the Loctite adhesive tolerated large deformation due to shear buckling of the adherend.

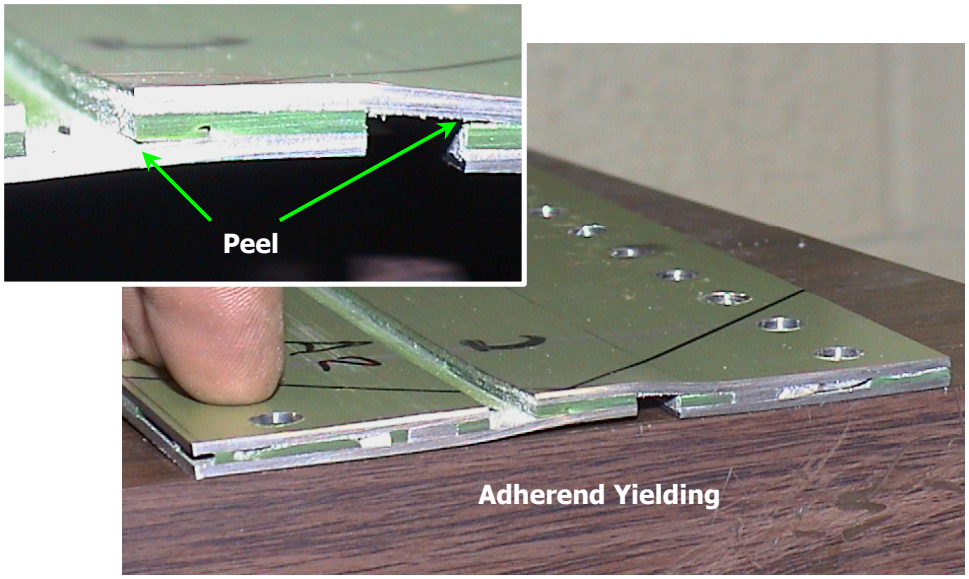

FIGURE 6-14. ALUMINUM ADHEREND YEILDING AND PEEL FAILURE

7. CONCLUSIONS.

The results of this investigation indicated that the shear-loaded lap joints decreased in strength as bondline thickness increased. This observation is analogous to results obtained for element level testing (ASTM D 1002, D 3165, and D 5656) conducted on adhesive single-lap shear testing. Analytical predictions using Shear-Loaded Bonded Joint (SLBJ) theory also represented this behavior due to the use of ASTM D 5656 single-lap shear coupon test data to model the constitutive behavior of adhesive by means of a two-parameter exponential curve. The rate of joint strength drop for increasing bondline thickness for SLBJ predictions was higher than that of experimental data. This resulted in conservative SLBJ predictions for thick bondlines. Linear regression for experimental data and SLBJ predictions indicated that the SLBJ predictions were 4.2%, 9.1%, 15.1%, and 22.4% lower than the average experimental data for bondline thickness of 0.05, 0.10, 0.16, and 0.20 inch, respectively. Thus, the SLBJ consistently showed conservative results with respect to the experimental data. Phase I test results also indicated changes in failure modes as the bondline thickness increased; thinner bondlines indicated substrate failure, and thicker bondlines indicated primarily cohesive failure. An accumulation of large plastic strains in thin bondlines resulted in high adherend interlaminar strains and caused substrate failure. The unstable damage development of thick bondlines resulted in adhesive cracking in multiple locations with a cohesive-type failure and lower failure strengths than that of the thin bondlines.

In Phase II, experimental data were substantially lower than the SLBJ predictions. In addition, both flat and joggle EA9360 specimens failed in the substrate, regardless of the bondline thickness. Low interlaminar shear strength of the adherend and plastic strain characteristics of the adhesive, compared to material used in Phase I, caused adherend failure of EA9360 joints rather than in the failure adhesive. This caused the SLBJ predictions to be lower than the experimental failure strength. These results, however, indicated a decrease in strength as bondline thickness increased, mainly because of the low yield strength of thick adhesives. In addition, joggle joint strength was somewhat higher than that of flat joints due to the additional surface area for adhesive bonding. ASTM D 5656 element tests indicated higher yield stress and better plastic strain accumulation of EA9360 adhesive compared to ES6292 adhesive. Nevertheless, the box beam subcomponent testing had demonstrated that the performance of the ES6292 joints was better than that of EA9360 joints. The failure analysis, however, revealed that this was due to the extensive shear strains accumulated by the stable damage development of EA9360 compared to ES6292 for this particular bondline thickness, which subsequently resulted in the interlaminar failure rather than in the failure adhesive.

Loctite specimens also indicated substrate failure due to significant shear buckling. The ductility of the adhesive permitted peel failure at the corners, but the joint continued to carry additional load. On the other hand, both ES6292 and EA9360 specimens failed catastrophically because of the brittle characteristics of these two adhesives. Even though the SLBJ predictions for Loctite specimens were comparable with experimental data, the comparison can be misleading due to the joint failure (substrate failure), rather than the adhesive failure mode as considered for theoretical predictions.

Efforts to investigate failure initiation using Electronic Speckle Pattern Interferometry (ESPI) or Photogrammetry (ARAMIS) were ineffective. The sensitivity of the ESPI system was unable to keep pace with the severe rigid body motion of torsion testing, and the sensitivity of the ARAMIS system was incapable of capturing any anomalies towards failure.

Experimental data in this investigation revealed the significance of adhesive characterization and the adhesive joint characterization with respect to the development of an analytical model. When predicting failure of the joint, one must pay attention to the failure mode because it largely contributes to the joint performance. Since SLBJ predictions were based on the adhesive plastic strain assuming linear elastic behavior of the adherend, the validity of these predictions were limited to the joints with cohesive failure in the adhesive with minimal nonlinearity of adherend materials. When these conditions were met, the SLBJ model showed good correlation with the experimental results.

8. REFERENCES.

1. Lee, J. and Kim, H., "The Prediction of Failure in In-Plane Shear Loaded Composite Bonded Joints," *Proceedings of the American Society for Composites 17th Technical Conference,* Purdue University, West Lafayette, IN, October 21-23, 2002.

2. Nguyen, V. and Kedward, K. T., "Non-Linear Modeling of Tubular Scarf Joints Loaded in Torsion," *Journal of Adhesion,* Vol. 76, 2001, pp. 265-92.

3. Kim, H. and Kedward, K. T., "Stress Analysis of Adhesive Bonded Joints Under In-Plane Shear Loading," *Journal of Adhesion*, Vol. 76, 2001, pp. 1-36.

4. Hibbitt, Karlsson & Sorensen, Inc., *ABAQUS 6.1 User's Manual*, Vol. 1, 2000.

5. Tomblin, J., Seneviratne, W., Escobar, P., and Yap, Y., "Shear Stress-Strain Data for Structural Adhesives," Federal Aviation Administration Report DOT/FAA/AR-02/97, November 2002.

6. Tomblin, J., McKenna, Y., Ng, Y., and Raju, K.S., "B-Basis Design Allowable for Epoxy-Based Prepreg: Newport E-Glass Fabric 7781/NB321," AGATE WP3.3-033051-097, NASA Langley Research Center, Hampton, VA, July 2001.

7. Tomblin, J., McKenna, Y., Ng, Y., and Raju, K.S., "B-Basis Design Allowable for Epoxy-Based Prepreg: Newport Carbon Plain Weave Fabric 3K70P/NB321," AGATE WP3.3-033051-095, NASA Langley Research Center, Hampton, VA, July 2001.

8. Tomblin, J., Seneviratne, W., Escobar, P., and Yap, Y., "Adhesive Behavior in Aircraft Applications," 2nd Annual FAA Centers of Excellence Meeting, Wichita, KS, October 21-24, 2002.

9. Megson, T.H.G., *Aircraft Structures for Engineering Students*, 2nd ed, Halsted Press, New York, 1990.

10. Tomblin, J., Harter, P., Seneviratne W., and Yang, C., "Characterization of Bondline Thickness Effects in Adhesive Joints," *ASTM Journal of Testing and Evaluation*, JCTRER, Vol. 24, No. 2, April 2002, pp. 332-44.

11. Tomblin, J., Yang, C., and Harter, P., "Investigation of Thick Bondline Adhesive Joints," Federal Aviation Administration Report, DOT/FAA/AR-01/33, June 2001.

12. Polymer Matrix Composites: Guidelines for Characterization of Structural Elements, Vol. 1, Working Draft, MIL-HDBK-17-1E, Department of Defense, pp. 7-44 – 7-61.

13. Yang, C. and Tomblin, J., "Investigation of Adhesive Behavior in Aircraft Applications," Federal Aviation Administration Report DOT/FAA/AR-01/57, September 2001.

APPENDIX A—BOX BEAM TORSION TEST FIXTURE (DETAILS)

The following drawings show the specimen with 1-inch gage width (Drawing UCSB-BB-030) and the 20-ply glass side panel (Drawing UCSB-BB-060). The 0.125-inch-thick aluminum plate, which replaced this 20-ply side plate, has identical hole patterns and dimensions, as shown in Drawing UCSB-BB-060.

Machining of the end plugs, steel channels, and test fixture was carried out at Wichita State University. The 0.125-inch-thick doubler plates (Drawing UCSB-BB-010) were added to the edges of the top and bottom inner walls, and the end plugs (Drawing UCSB-BB-010) were altered to accommodate additional material.

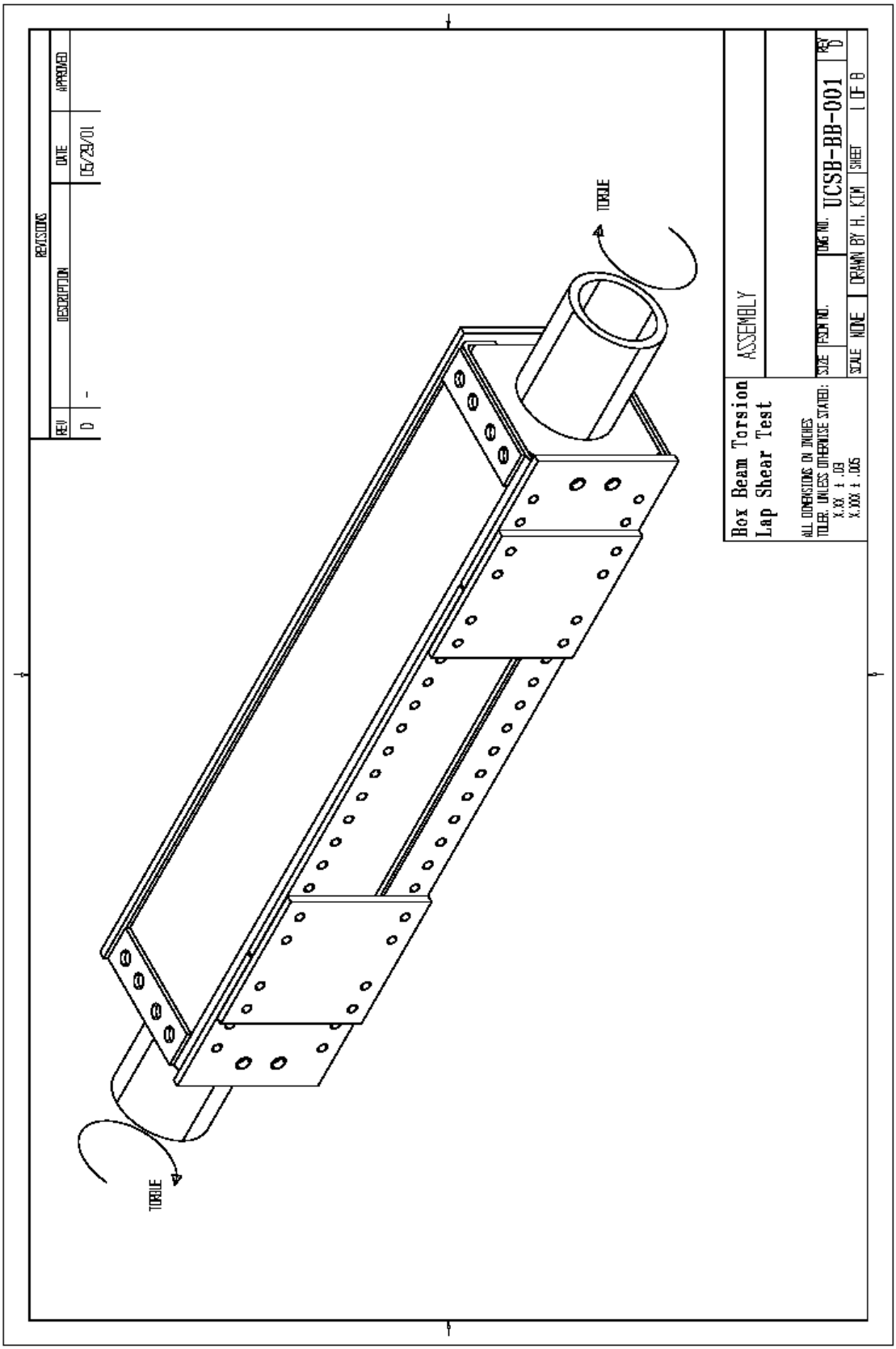
REVISIONS
REV
DESCRIPTION
DATE
APPROVED
0
-
05/29/01
TORQUE
TORQUE
Box Beam Torsion
Lap Shear Test
ASSEMBLY
ALL DIMENSIONS ON INCHES
TOLER. UNLESS OTHERWISE STATED:
X.XX ± .03
X.XXX ± .005
SIZE
FSCM NO.
DWG NO.
UCSB-BB-001
REV
D
SCALE NONE
DRAWN BY H. KIM
SHEET 1 OF 8

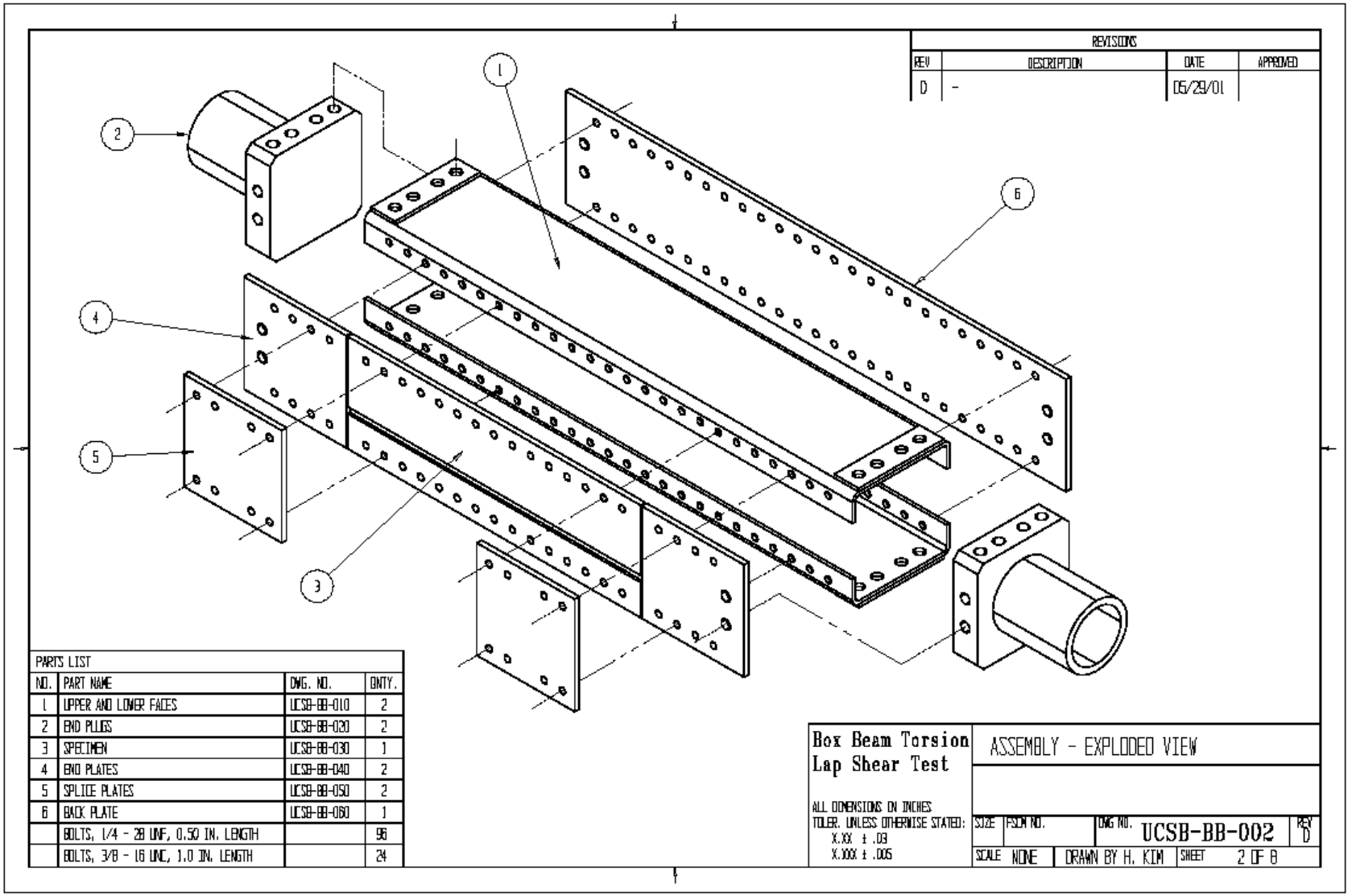
REVISIONS
REV | DESCRIPTION | DATE | APPROVED
D | - | 05/29/01
1
2
3
4
5
6
PARTS LIST
NO. | PART NAME | DWG. NO. | QNTY.
1 | UPPER AND LOWER FACES | UCSB-BB-010 | 2
2 | END PLUGS | UCSB-BB-020 | 2
3 | SPECIMEN | UCSB-BB-030 | 1
4 | END PLATES | UCSB-BB-040 | 2
5 | SPLICE PLATES | UCSB-BB-050 | 2
6 | BACK PLATE | UCSB-BB-060 | 1
BOLTS, 1/4 - 28 UNF, 0.50 IN. LENGTH | | 96
BOLTS, 3/8 - 16 UNC, 1.0 IN. LENGTH | | 24
Box Beam Torsion Lap Shear Test
ASSEMBLY - EXPLODED VIEW
ALL DIMENSIONS IN INCHES
TOLER. UNLESS OTHERWISE STATED:
X.XX ± .03
X.XXX ± .005
SIZE | FSCM NO. | DWG NO. UCSB-BB-002 | REV D
SCALE NONE | DRAWN BY H. KIM | SHEET 2 OF 8

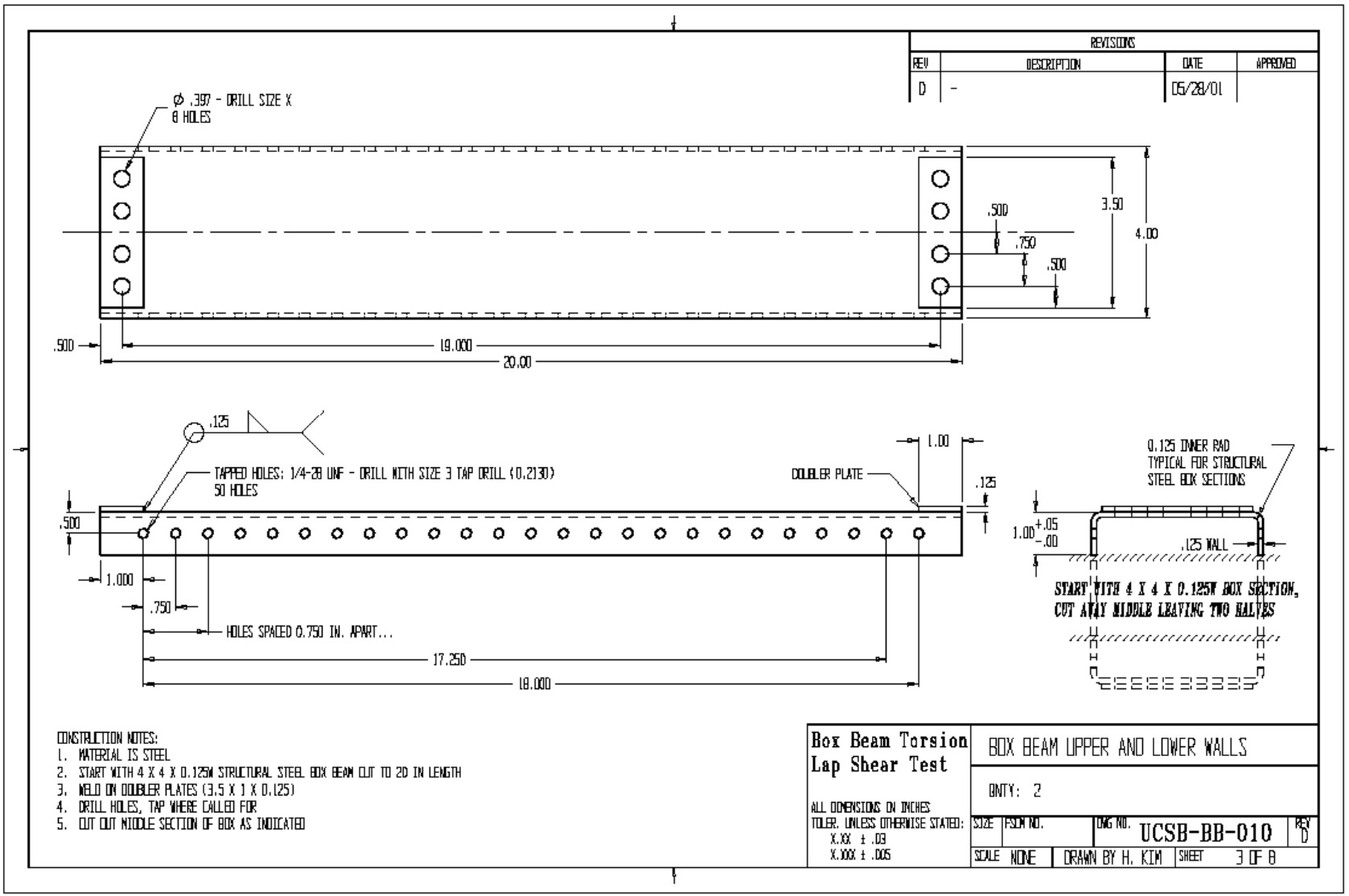
REVISIONS
REV | DESCRIPTION | DATE | APPROVED
D | - | 05/28/01
Ø .397 - DRILL SIZE X
8 HOLES
.500
3.50
4.00
.750
.500
.500
19.000
20.00
.125
TAPPED HOLES: 1/4-28 UNF - DRILL WITH SIZE 3 TAP DRILL (0.2130)
50 HOLES
DOUBLER PLATE
1.00
.125
.500
1.000
.750
HOLES SPACED 0.750 IN. APART...
17.250
18.000
0.125 INNER RAD
TYPICAL FOR STRUCTURAL
STEEL BOX SECTIONS
1.00 +.05 -.00
.125 WALL
START WITH 4 X 4 X 0.125W BOX SECTION,
CUT AWAY MIDDLE LEAVING TWO HALVES
CONSTRUCTION NOTES:
1. MATERIAL IS STEEL
2. START WITH 4 X 4 X 0.125W STRUCTURAL STEEL BOX BEAM CUT TO 20 IN LENGTH
3. WELD ON DOUBLER PLATES (3.5 X 1 X 0.125)
4. DRILL HOLES, TAP WHERE CALLED FOR
5. CUT OUT MIDDLE SECTION OF BOX AS INDICATED
Box Beam Torsion
Lap Shear Test
ALL DIMENSIONS IN INCHES
TOLER. UNLESS OTHERWISE STATED:
X.XX ± .03
X.XXX ± .005
BOX BEAM UPPER AND LOWER WALLS
QNTY: 2
SIZE
FSCM NO.
DWG NO. UCSB-BB-010
REV D
SCALE NONE
DRAWN BY H. KIM
SHEET 3 OF 8

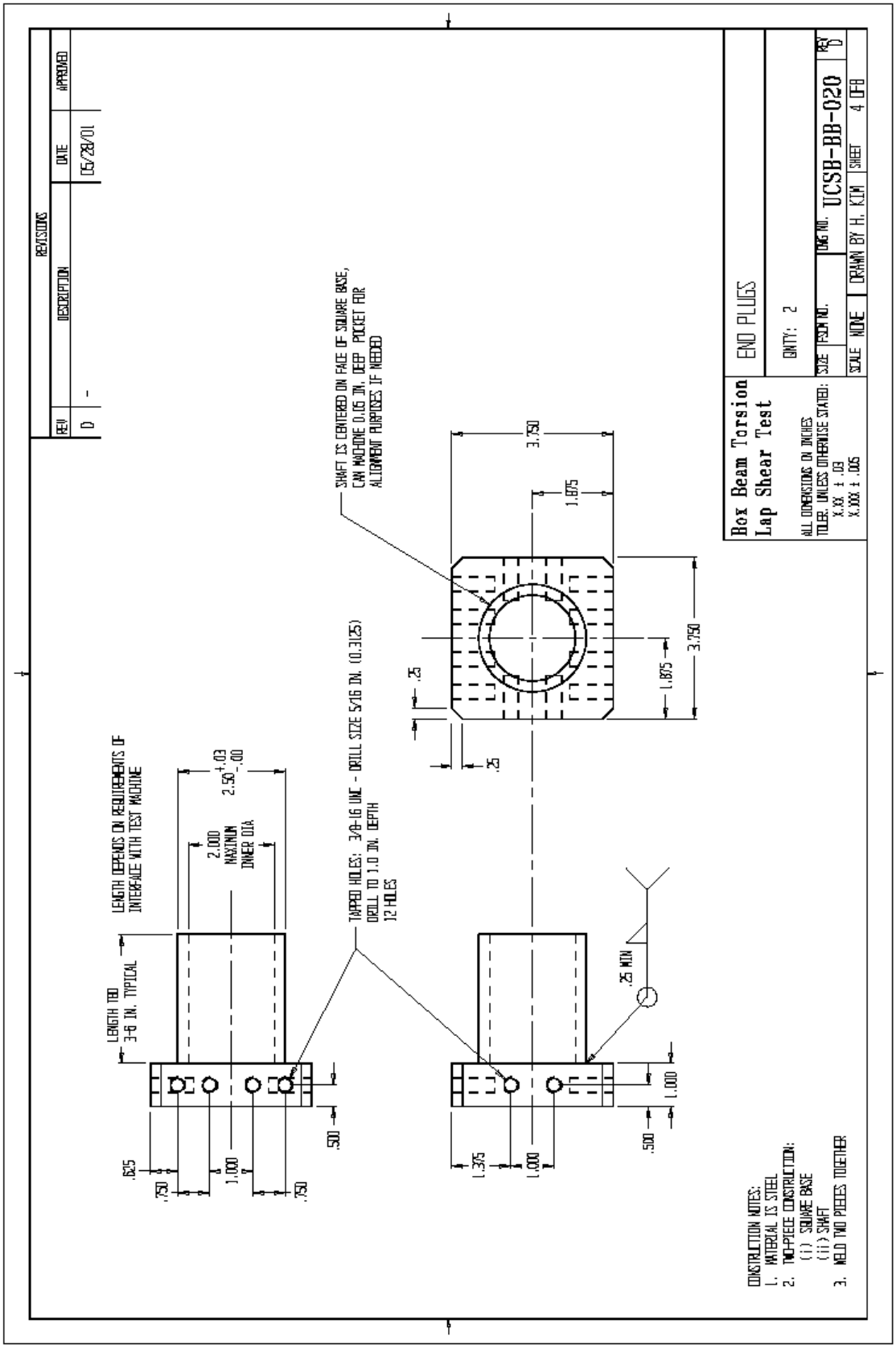
REVISIONS
REV
DESCRIPTION
DATE
APPROVED
D
-
05/29/01
Box Beam Torsion
Lap Shear Test
END PLUGS
QNTY: 2
ALL DIMENSIONS IN INCHES
TOLER. UNLESS OTHERWISE STATED:
X.XX ± .03
X.XXX ± .005
SIZE
FSCM NO.
DWG NO.
UCSB-BB-020
REV
D
SCALE NONE
DRAWN BY H. KIM
SHEET 4 OF 8
SHAFT IS CENTERED ON FACE OF SQUARE BASE,
CAN MACHINE 0.05 IN. DEEP POCKET FOR
ALIGNMENT PURPOSES IF NEEDED
LENGTH DEPENDS ON REQUIREMENTS OF
INTERFACE WITH TEST MACHINE
LENGTH TBD
3-6 IN. TYPICAL
TAPPED HOLES: 3/8-16 UNC - DRILL SIZE 5/16 IN. (0.3125)
DRILL TO 1.0 IN. DEPTH
12 HOLES
2.000
MAXIMUM
INNER DIA
2.50 +.03 -.00
3.750
1.875
.25
.25 MIN
.625
.750
1.000
.750
.500
1.375
1.000
.500
CONSTRUCTION NOTES:
1. MATERIAL IS STEEL
2. TWO-PIECE CONSTRUCTION:
(i) SQUARE BASE
(ii) SHAFT
3. WELD TWO PIECES TOGETHER

REVISIONS			
REV	DESCRIPTION	DATE	APPROVED
D	-	05/28/01	

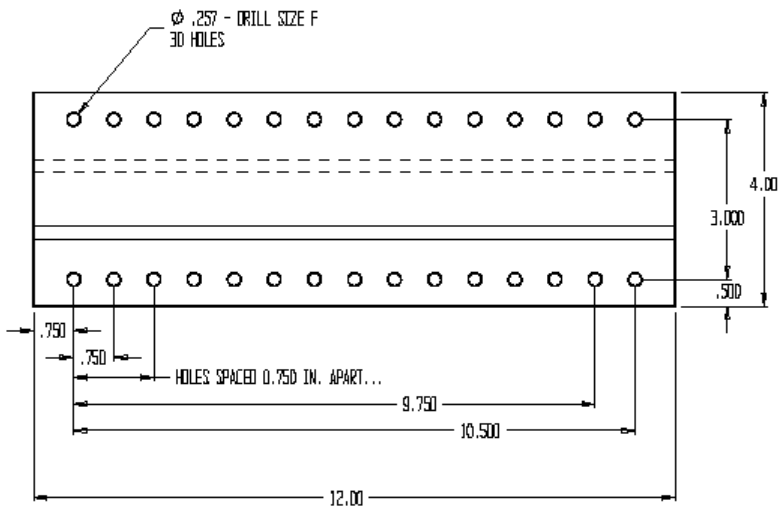

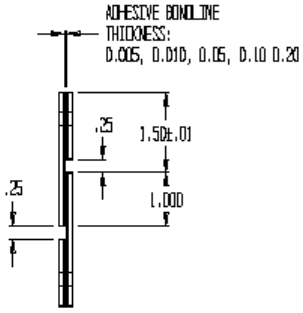

CONSTRUCTION NOTES:
1. MATERIAL IS GLASS/EPOXY CLOTH OF 10 PLIES [0_4/45/-45/0_4] LAYUP
2. BOND PANELS TOGETHER AT DESIRED BONDLINE THICKNESS
3. CUT SPECIMENS TO GLOBAL DIMENSIONS - 12 X 4 IN.
4. MACINE SLOTS TO FORM LAP JOINTS, SIMILAR TO ASTM D3163
5. DRILL HOLES - ONLY 30

Box Beam Torsion Lap Shear Test	SPECIMEN			
	QNTY: SEE TEST MATRIX			
ALL DIMENSIONS IN INCHES TOLER. UNLESS OTHERWISE STATED: X.XX ± .03 X.XXX ± .005	SIZE	FSCM NO.	DWG NO. UCSB-BB-030	REV D
	SCALE NONE	DRAWN BY H. KIM	SHEET 5 OF 8	

REVISIONS			
REV	DESCRIPTION	DATE	APPROVED
D	-	05/29/01	

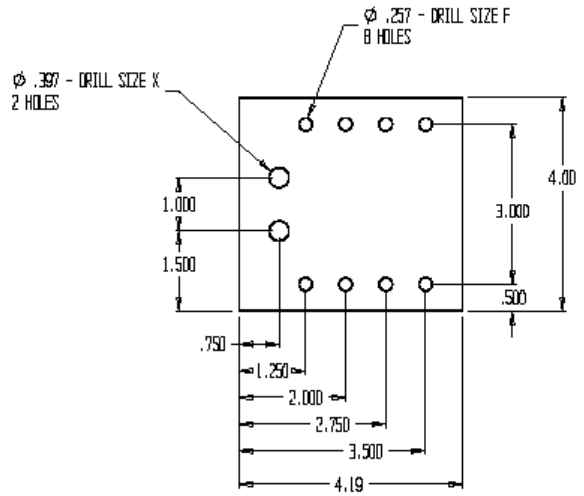

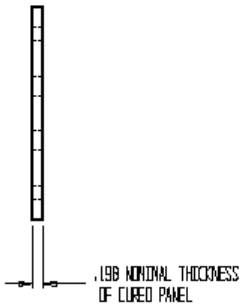

CONSTRUCTION NOTES:
1. MATERIAL IS GLASS/EPOXY CLOTH OF 20 PLIES [0_4/45/-45/0_B/-45/45/0_4] LAYUP

Box Beam Torsion Lap Shear Test	END PLATES			
	QNTY: 2			
ALL DIMENSIONS IN INCHES TOLER. UNLESS OTHERWISE STATED: X.XX ± .03 X.XXX ± .005	SIZE	FSCM NO.	DWG NO. UCSB-BB-040	REV D
	SCALE NONE	DRAWN BY H. KIM	SHEET 6 OF 8	

REVISIONS			
REV	-	DATE	APPROVED
D	ENTER DESCRIPTION	05/28/01	

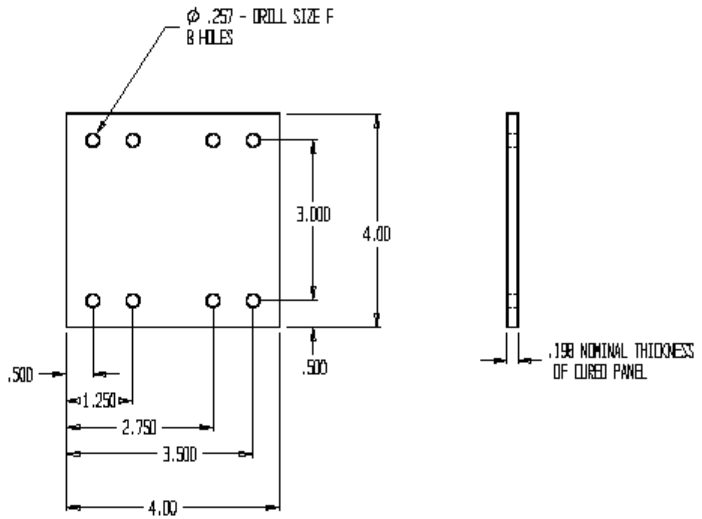

CONSTRUCTION NOTES:
1. MATERIAL IS GLASS/EPOXY CLOTH OF 20 PLIES [0_4/45/-45/0_8/-45/45/0_4] LAYUP

Box Beam Torsion Lap Shear Test	SPLICE PLATES			
	QNTY: 2			
ALL DIMENSIONS IN INCHES TOLER. UNLESS OTHERWISE STATED: X.XX ± .03 X.XXX ± .005	SIZE	FSCM NO.	DWG NO. UCSB-BB-050	REV D
	SCALE NONE	DRAWN BY H. KIM	SHEET 7 OF 8	

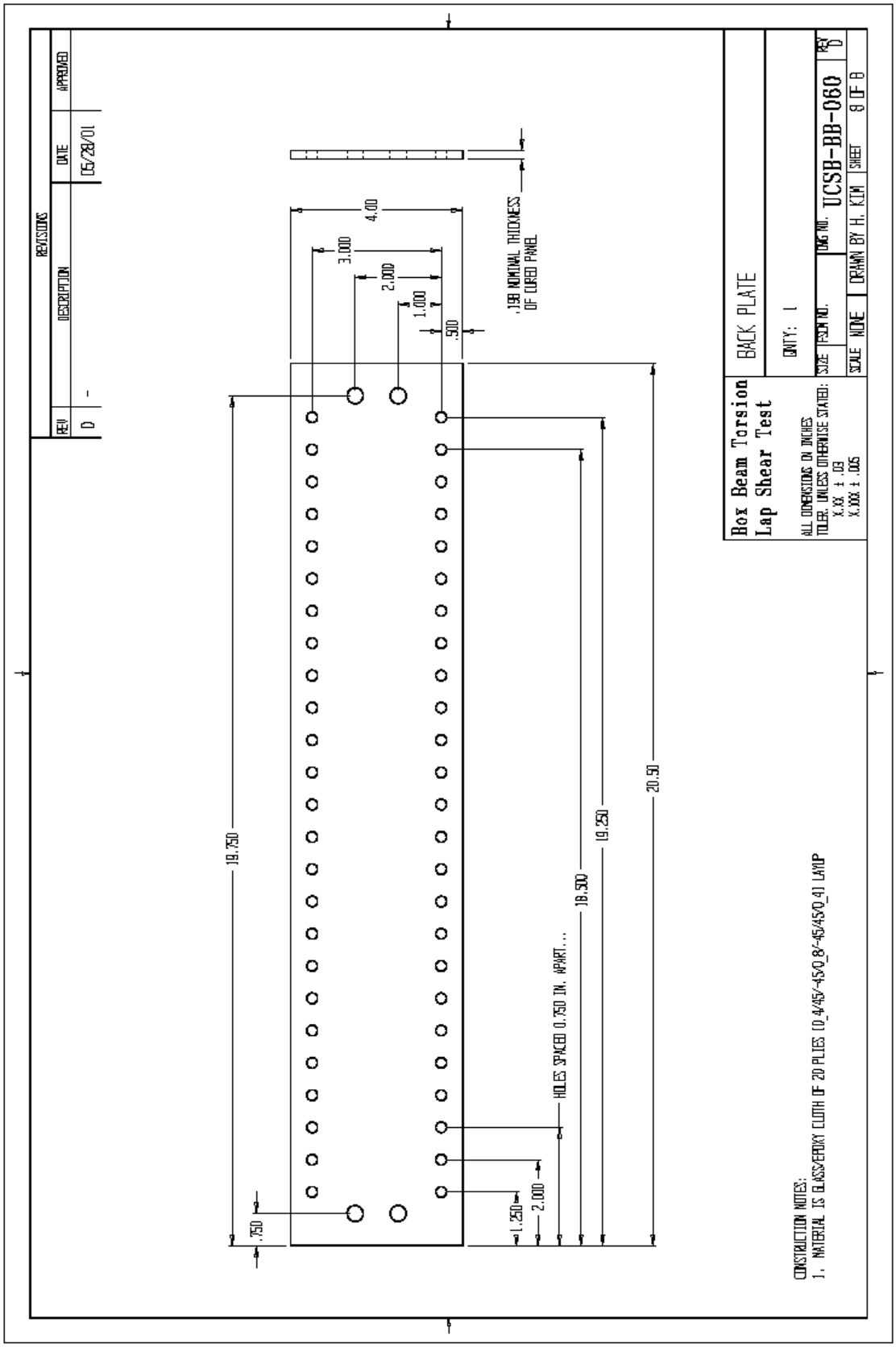
REVISIONS
REV
DESCRIPTION
DATE
APPROVED
D
-
05/29/01
4.00
3.000
2.000
1.000
.930
.198 NOMINAL THICKNESS
OF CURED PANEL
19.750
.750
1.250
2.000
HOLES SPACED 0.750 IN. APART...
18.500
19.250
20.50
CONSTRUCTION NOTES:
1. MATERIAL IS GLASS/EPOXY CLOTH OF 20 PLIES [0/45/-45/0/-45/45/0]_4T LAYUP
Box Beam Torsion
Lap Shear Test
BACK PLATE
QNTY: 1
ALL DIMENSIONS IN INCHES
TOLER: UNLESS OTHERWISE STATED:
X.XX ± .03
X.XXX ± .005
SIZE
FSCM NO.
DWG NO.
UCSB-BB-060
REV
D
SCALE NONE
DRAWN BY H. KIM
SHEET
8 OF 8